INCLUSIONS IN VACUUM INDUCTION MELTED NICKEL-BASE ALLOYS

by

David Walter Gusching

A Thesis Submitted to the Faculty of the

DEPARTMENT OF METALLURGICAL ENGINEERING

In Partial Fulfillment of the Requirements
For the Degree of

MASTER OF SCIENCE

In the Graduate College

THE UNIVERSITY OF ARIZONA

1 9 8 1

STATEMENT BY AUTHOR

This thesis has been submitted in partial fulfillment of requirements for an advanced degree at The University of Arizona and is deposited in the University Library to be made available to borrowers under rules of the Library.

Brief quotations from this thesis are allowable without special permission, provided that accurate acknowledgment of source is made. Requests for permission for extended quotation from or reproduction of this manuscript in whole or in part may be granted by the head of the major department or the Dean of the Graduate College when in his judgment the proposed use of the material is in the interests of scholarship. In all other instances, however, permission must be obtained from the author.

SIGNED: David W. Gusching

APPROVAL BY THESIS DIRECTOR

This thesis has been approved on the date shown below:

David R. Poirier

DAVID R. POIRIER
Associate Professor of Metallurgical Engineering

2/12/81

Date

ACKNOWLEDGMENTS

The author wishes to thank his advisor, Dr. David Poirier, for his guidance and helpful suggestions throughout this work. Sincere thanks are extended to Mr. Tom Teska for his help on the microprobe unit. The microprobe time granted by Dr. Michael Drake is also appreciated. The help of Dr. Kenneth Keating and Dr. Louis Demer was also appreciated. The financial assistance for this author was provided by an HEW Mining and Mineral Fuel Conservation Fellowship.

TABLE OF CONTENTS

TABLE OF CONTENTS--Continued

LIST OF ILLUSTRATIONS

LIST OF ILLUSTRATIONS--Continued

LIST OF TABLES

LIST OF TABLES--Continued

ABSTRACT

The reactions which lead to the formation of harmful primary inclusions in nickel-base alloys are analyzed in this study. Twelve heats were melted and cast in a vacuum induction melting unit. Alloys containing Ni-0.15C, Ni-0.15C-5Al, Ni-0.15C-1Hf, and Ni-0.15C-5Al-1Hf were melted in Al_2O_3, MgO, and ZrO_2 crucibles. Metallographic and microprobe analyses were performed on the twelve ingots and the three crucibles.

Hafnium oxide (HfO_2)-rich inclusions form on the bottom surfaces of all hafnium-bearing ingots. Alumina (Al_2O_3)-rich inclusions form on the top of all aluminum-bearing ingots. Differences among the skulls found on the three different types of crucibles were also noted. Specifically, an HfO_2 coating formed on the ZrO_2 crucible which was present during melting and remained as a tightly adhered skull after pouring. A nickel base skull which was not present during melting but formed during pouring adhered to the Al_2O_3 crucible. When melting in MgO, there was no appreciable coating or skull which formed on the MgO crucible. This phenomenon is explained in terms of the alloy's tendency not to wet the MgO crucible.

A summary of the major chemical reactions involved in the formation of harmful inclusions is presented.

CHAPTER 1

INTRODUCTION

1.1 Purpose of this Investigation

The chemical reactions which lead to the formation of oxide inclusions in nickel-base superalloys have not been researched in great detail. Nickel-base superalloys have many high-temperature applications such as turbine blades in aircraft engines. Inclusions in such parts must be kept to a minimum since they lower the strength and fatigue properties of the alloy and can cause catastrophic failures. Nickel-base superalloys are vacuum induction melted primarily because they contain several reactive elements and because impurity gaseous elements such as oxygen, hydrogen, and nitrogen can be reduced to levels unattainable by standard air-melting techniques. However, it has been suggested that crucible decomposition occurs at very low oxygen pressures, and this decomposition is a source for oxygen which enters the melt. Therefore, the purpose of this work is to identify and analyze the chemical reactions which cause harmful primary oxide inclusions to form in nickel base alloys during vacuum induction melting.

1.2 Background Information on Nickel Base Superalloys

According to Schlatter (1972), superalloys may be broadly defined as alloys with excellent oxidation resistance for service at high stress levels at temperatures exceeding 650°C (1200°F). Some of these alloys

also exhibit resistance to hot corrosion, and they are used extensively in high-temperature chemical processing equipment.

The development of nickel-base superalloys began in the late 1930's in Western Europe and the United States. As stated by Fawley (1972), the Mond Nickel Co. (now INCO) produced Nimonic alloy 75 in late 1941 for creep resistance for a British aircraft company; eventually they developed other superalloys. These alloys replaced the austenitic stainless steels then used. By the late 1940's, Waspaloy, Inconel, Hastelloy, René, and various other alloy series were being developed.

Vacuum induction melting of nickel-base alloys began in the early 1950's when the Kelsey-Hayes Company (and somewhat later Special Metals Co.) dramatically improved the quality and properties of the existing nickel-base alloys with this process. According to Fawley (1972), examples of commercial alloys which are typically vacuum induction melted include Waspaloy, René 41, Inconel 718, Udimet 500, D-797 and A-286. Vacuum induction melting is the general practice for forging stock and for investment castings of many nickel-base alloys.

1.3 Physical Metallurgy of Nickel Base Superalloys

Aluminum, hafnium, and carbon are the alloying elements used in this work. The reasons for adding these three alloying elements will be discussed.

As stated by Harris et al. (1977), superalloys have good high-temperature stress-rupture properties and relatively low density. The superalloys are principally hardened by a relatively high volume fraction

of Ni_3Al (γ') precipated in the f.c.c. (γ) matrix. This Ni_3Al phase is coherent with the nickel matrix because their lattice parameters are almost identical. Such alloys can be used at temperatures up to 80% of their absolute melting temperature range for long periods of time; this service temperature range is around 1800°F. The stress-rupture properties of the alloy depend on the volume fraction of the Ni_3Al phase; thus, high temperature stress-rupture properties depend on the amount of aluminum in the alloy.

Hafnium is added to superalloys to increase ductility and improve the consistency of the mechanical properties. Hockin (1972) states that the effect of cooling rates is reduced to the extent that good and consistent properties can be obtained almost independent of the section thickness. The addition of hafnium to nickel-base alloys radically changes the composition of the γ' in the eutectic. This is accomplished by the substitution of hafnium in the MC carbides for titanium and zirconium resulting in a higher titanium and zirconium content in the γ' than usual. The addition of hafnium to a high titanium nickel-base alloy produces a higher or non-optimum titanium content in the γ' causing a drop in mechanical properties. Thus, when hafnium is added, the titanium content of the overall alloy must be decreased.

Small amounts of carbon are added to each melt in this study; all superalloys have small amounts of carbon added. Carbon combines with elements like hafnium, titanium, and zirconium to form carbides. These carbides tend to improve the tensile properties of the superalloys. Carbon is also added for the purpose of deoxidizing the melt.

1.4 Vacuum Induction Melting of Superalloys

According to Schlatter (1972), vacuum induction melting has various advantages over other industrial melting techniques. Vacuum induction melting provides very flexible operation in absence of air and the best control over the entire melt chemistry, particularly when the melts contain reactive elements. Precise compositions can be reproduced from heat to heat; for some elements, the accuracy approaches the limits of present analytical techniques. Control of vacuum pressure permits exceptional degassing, strong carbon deoxidation, and favorable reaction kinetics. The use of induction stirring promotes rapid mass transfer of reactants to the melt-vacuum interface, excellent melt homogenization and quick dissolution of alloy additions. For these reasons, nickel base superalloys are commercially melted by vacuum induction melting, and this process was selected to melt the alloys in this study.

1.5 Choice of Crucibles for Melting Superalloys

Sutton and Maurer (1979) have discussed the many factors involved in the selection of a crucible; chemical stability, thermal properties, cost, and availability are major factors. Alumina (Al_2O_3) is widely used because of its availability, cost, and stability under vacuum. Magnesia (MgO) is also widely used by primary melters but not by foundries; however, it dissociates more readily than alumina. Zirconia (ZrO_2) which is more stable than alumina or magnesia is also used; however, it is very expensive.

According to Snape and Beeley (1967), melting refractories react, to some extent, with the alloy being melted; as a result, the

alloy is contaminated. They also state that crucible materials are responsible for a high percentage of nonmetallic inclusions in nickel-base superalloys. Vaughn and Geiger (1979) state that decomposition of the crucible is a source of oxygen in the melt. Oxygen reacts with reactive elements such as aluminum and hafnium in the melt to form Al_2O_3 and HfO_2 inclusions, respectively.

In this work, Al_2O_3, MgO, and ZrO_2 crucibles were used to melt a number of nickel-base alloys under vacuum induction melting conditions, and the characteristics of each crucible under vacuum melting conditions was studied.

1.6 Inclusions and Harmful Effects

Inclusions are nonmetallic impurities which exist in a metallic matrix; they can result during solidification and/or during melting. Emphasis in this study is on primary inclusions which are those inclusions formed prior to the solidification of the primary solid.

Hockin (1972) states that hafnium oxide is seen, basically, in three different stages. The first stage, where major hafnium oxide inclusions are present, may be detected by nondestructive tests normally employed on cast components such as radiography and penetrants which fluoresce under ultraviolet light. These are easily detected by radiography due to their density. The second stage of hafnium oxide is where platelets are dispersed throughout the microstructure; these fine oxide inclusions are not detectable by normal nondestructive tests carried out on production castings. The third form of hafnium oxide, which is

observed as a very fine Chinese script-like precipitate, is not normally considered detrimental.

Flemings (1974) states that in steel melts large interconnected clusters of alumina (Al_2O_3) inclusions form which contain hundreds of individual inclusions. Primary alumina inclusions (in steel) are generally more angular in appearance as opposed to spherical SiO_2 inclusions. Vaughn and Geiger (1979) report that Al_2O_3 clusters can also form in nickel-base melts. In a cluster small primary Al_2O_3 particles appeared to have agglomerated, with the result that a much larger volume of metal is affected than would be if the particles were dispersed. Vaughn and Geiger (1979) also report that clouds of alumina or scum (dross) formed on the top of the melts as well as, quite logically, on the top of the solidified ingots.

Inclusions can be a severe problem for the manufacturers of nickel-base superalloy castings. For example, Marder (1979) states that turbine blades cast of directionally-solidified MAR-M200 + Hf had many inclusions and dross defects. The author believes that the dross effects occurred primarily because of refractory-metal reactions; this was the single major cause for rejection of these blades and accounted for over 90% of castings rejected by a fluorescent penetration inspection. The tensile and stress-rupture properties were not significantly affected except at extreme dross levels. However, low-cycle fatigue and creep-rupture properties were reduced considerably even at mild defect levels as shown by Marder (1979) in Table 1. The effect of dross severity on low-cycle fatigue life is plotted by Mosier (1978) in Figure 1.

Table 1. Effect of dross severity on low-cycle fatigue life of directionally-solidified MAR M200 + Hf (Marder, 1979).

Dross Severity Rating	Maximum Defect Size (inches)	Fatigue Life @ 1800°F (982°C) 0-50 ksi (cycles)
None	0.01	6137
Mild	0.01-0.03	3970
Intermediate	0.03-0.5	2342
Severe	0.5	1500

Another study by Sakakibara and Sekino (1972) showed that the hot workability of nickel-base alloys is reduced by inclusions. This is very important because these alloys are often forged into useful products.

1.7 Overview of This Study

A series of 12 nickel-base melts was made in a vacuum induction melting furnace. Alloys with various compositions of nickel, aluminum, hafnium, and carbon were melted in crucibles of three different types; the three crucibles were Al_2O_3, MgO, and ZrO_2. After melting, the liquid metal was poured into a silica sand mold to form an ingot. The ingots and the crucibles were then sectioned; pieces from representative sections of the ingots and crucibles were prepared for metallographic examination and microprobe analyses. Microprobe compositions, x-ray distribution images, as well as secondary electron pictures of primary inclusions and crucible sections were obtained by using the microprobe. From these results, much was learned about the chemical reactions which take place to form inclusions.

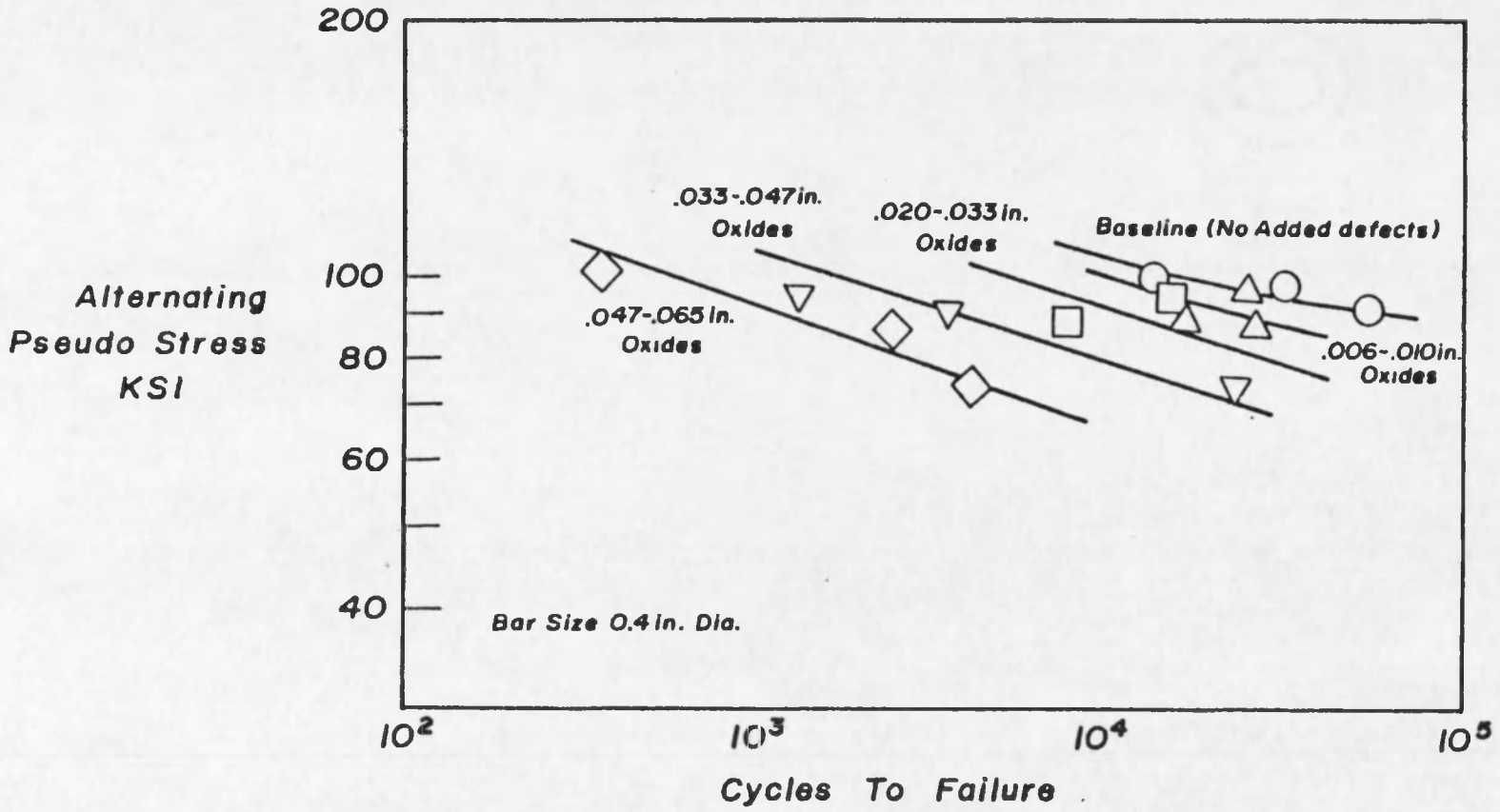

Fig. 1. Effect of oxide inclusions on the LCF characteristics of HIP'ed Rene' 95 powder (Mosier, 1978).

CHAPTER 2

THEORY OF INCLUSION FORMATION

2.1 Overview of Formation of Inclusions

Inclusions are nonmetallic particles in a metallic matrix which form during melting and/or solidification of castings. The formation of primary oxide inclusions is emphasized in this chapter, and thermodynamic data pertinent to inclusion formation are presented to explain the chemical reactions involved in the formation of inclusions.

Oxide inclusions form due to various sources of oxygen which are present when nickel is processed by vacuum induction melting. Major sources include the oxides of the refractory materials, oxygen in the chamber atmosphere (typically 1-10 microns pressure), and oxygen in the charge materials. When these charge materials are heated and melted, oxygen from the chamber atmosphere as well as from the decomposing crucibles can be absorbed into the melt. After at least one melt has been made in a crucible, other oxide sources become present. The alloy which remains after pouring and forms a "skull" on the crucible is a source of inclusions. Also, the metal condensate above the melt line can oxidize between melts and introduce oxides in subsequent melts.

Oxygen from the various sources reacts with deoxidizing elements in the melts such as carbon, aluminum, and hafnium as well as elements which are from decomposing refractories, such as zirconium, magnesium, silicon, and calcium. Some of the more stable oxides (e.g., Al_2O_3, MgO,

and ZrO_2) form within the melt and tend to float to the top surface of castings and form dross defects; these oxides are less dense than the nickel-base alloy. Hafnium oxide can also form in the melt, and because it is more dense than the nickel-base alloy, it sinks to the bottom of the melt and is concentrated on the bottom surfaces of castings.

2.2 Thermodynamic Considerations

Chemical reactions in any metal system can be better understood if the thermodynamics of the system are analyzed. Data on thermodynamic properties in nickel-base melts are available in a paper by Sigworth et al. (1977). Calculated deoxidation equilibria in nickel alloys of interest are presented in Table 2; the equilibrium constants are for 1550°C which is the pouring temperature of the melts in this study. Raoultian activity coefficients of elements in dilute solution are presented in Table 3. The standard state used for the data in this table is the Henrian standard state.

These data can be used to predict the direction of chemical reactions in nickel-base melts. For example, consider the reaction:

$$MO_x(s) + x\underline{N} = \underline{M} + xNO \qquad (1)$$

The free energy of this reaction can be calculated by

$$\Delta G = x\Delta G^\circ_{NO} - \Delta G^\circ_{MO_x} + RT \ln \frac{a_{\underline{M}}}{a^x_{\underline{N}}} \qquad (2)$$

where ΔG is the free energy of the reaction. The values ΔG°_{MO} and ΔG°_{NO} represent the standard free energy of formation of the two oxides. The

Table 2. Calculated deoxidation equilibria in nickel alloys (Sigworth et al. 1977).

Deoxidation Reaction	log K	$K_{1550°C}$
$2\,\underline{Al} + 3\underline{O} = Al_2O_3(s)$	60,760/T - 18.7	4.262×10^{14}
$\underline{C} + \underline{O} = CO(g)$	3,230/T + 2.26	1.075×10^{4}
$\underline{Ca} + \underline{O} = CaO(s)$	27,706/T - 6.57	4.246×10^{8}
$\underline{Mg} + \underline{O} = MgO(s)$	26,324/T - 7.57	7.411×10^{6}
$\underline{Si} + 2\underline{O} = SiO_2(s)$	32,980/T - 10.88	1.625×10^{7}
$\underline{Zr} + 2\underline{O} = ZrO_2(s)$	34,000/T - 7.52	1.350×10^{11}

Table 3. Raoultian activity coefficients of elements in dilute solution (Sigworth et al. 1977).

Element	γ 1600°C
Al (l)	0.00025
C (s)	0.31
Ca (l)	0.6
Mg (l)	0.32
Si (l)	0.00014
Zr (s)	0.00007

values $a_{\underline{M}}$ and $a^{x}_{\underline{N}}$ represent the activity of the metallic element in solution, T is absolute temperature, and R is the gas constant.

The free energy of formation of the oxides can be calculated using Eq. (3); the values of K at 1550°C (1823°K) are listed in Table 2 for various oxides.

$$\Delta G^{\circ} = - RT \ln K \tag{3}$$

The value K represents the equilibrium constant.

The conversion factor shown below must be used to convert activities from the Raoultian activity scale to the Henrian scale.

$$\frac{a_{\underline{M}\ \text{Raoult}}}{a_{\underline{M}\ \text{wt \%}}} = \frac{\gamma^{\circ}_{\underline{M}}\, M_{\underline{M}}}{100 M_{\underline{wi}}} \tag{4}$$

Care must be taken in the treatment of the data because thermodynamics can only be used to predict the direction of chemical reactions. The kinetics or rates of reaction cannot be determined from thermodynamics.

2.3 Chemical Reactions at the Melt-Crucible Interface

This discussion of the chemical reactions which form inclusions is divided into two sections to simplify the explanation. The first section deals with reactions at the melt-crucible interface and the second section deals with reactions within the melt and at the melt-vacuum interface.

It is widely known that reduction of the refractory by carbon takes place during vacuum induction melting. It is theorized that this is a two step process; the crucible decomposes and the free oxygen reacts with carbon to form CO(g). For example, an MgO crucible decomposes by the reaction:

$$MgO(s) \rightarrow Mg(g) + \underline{O} \tag{5}$$

This free oxygen reacts with carbon to form CO(g) as follows:

$$\underline{C} + \underline{O} \rightarrow CO(g) \tag{6}$$

It is evident that the overall reaction is:

$$MgO(s) + \underline{C} \rightarrow Mg(g) + CO(g) \tag{7}$$

However, bubbles of Mg and CO form only near the melt surface because the metallostatic head suppresses gas bubbles at greater depths. For example, Vaughn and Geiger (1979) calculated that bubbles containing CO and Mg vapor (MgO crucibles used) could form down to 0.5 cm below the surface of a melt containing 0.01 wt. % carbon with a total pressure of 5×10^{-3} atm. Reactions (8) - (13) are other examples of reactions between carbon in the melt and various refractory materials.

$$ZrO_2(s) + 2\underline{C} = \underline{Zr} + 2CO(g) \tag{8}$$

$$CaO(s) + \underline{C} = \underline{Ca} + CO(g) \tag{9}$$

$$SiO_2(s) + 2\underline{C} = \underline{Si} + 2CO(g) \tag{10}$$

$$Al_2O_3(s) + 2\underline{C} = Al_2O(g) + 2CO(g) \tag{11}$$

$$Al_2O_3(s) + \underline{C} = 2AlO(g) + CO(g) \quad (12)$$

$$Al_2O_3(s) + 3\underline{C} = 2\underline{Al} + 3CO(g) \quad (13)$$

Although the reaction of carbon with a refractory oxide does not directly introduce oxygen into the melt, this carbon does not react with oxygen already in the melt to form harmless CO bubbles. Thus, the effect of carbon as a deoxidizer is diminished by carbon-refractory reactions.

It is evident that reactions (7) - (10) go in the forward direction because initially there is no Mg, Zr, Ca, or Si (activity = 0) in the nickel-base melts. Thus, to approach equilibrium, the crucibles must decompose at least to some slight extent. Calcium and silicon in the melt are considered because there is CaO and SiO_2 in the MgO and ZrO_2 crucibles.

To show how favorable these reactions are at typical vacuum pressures, reaction (7) was analyzed by Vaughn and Geiger (1979). They state that in the presence of as little as 0.001 wt. % C or more, the pressure of CO(g) and Mg(g) from the reaction are greater than 0.8 torr each for a total pressure of 1.6 torr. This means that the reaction will proceed to the right when the total pressure is less than 0.6 torr (1600 microns) for % C $\geq$ 0.001%; typical vacuum melting pressures are 1-10 microns. Thus, the beneficial effects of melting under a strong vacuum are offset by crucible decomposition and, in fact, Vaughn and Geiger (1979) suggest that melting should be done at pressures greater than normally used.

The reaction between Al_2O_3 and carbon results in partial pressures of $Al_2O(g)$, AlO(g), and Al(g); their respective values depend on the

equilibrium constants for reactions (11) - (13). Meadowcraft and Elliott (1963) state that these vapor species which form under vacuum conditions diminish the effectiveness of substituting more stable oxides for Al_2O_3 as a crucible material. In other words, the oxygen is not introduced into the melt where it can react to form inclusions. Instead, it is in the form of gases above the melt.

Also, the crucibles can decompose at low pressures in the absence of carbon. Examples of these include the reactions listed below:

$$MgO(s) = \underline{Mg} + O \tag{5}$$

$$Al_2O_3(s) = Al_2O(g) + 2\underline{O} \tag{14}$$

$$ZrO_2(s) = \underline{Zr} + 2\underline{O} \tag{15}$$

These reactions are favored at low pressures (or low $\underline{O}$ content) in the molten metal. Thus, oxygen supplied to the melt from the decomposing crucible offsets the oxygen which leaves the melt surface and is pumped away by the vacuum pump.

Oxide layers can form preferentially on the crucibles in certain melt-refractory combinations. These form when an alloy element in the melt is favored thermodynamically to reduce the refractory oxides. Snape and Beeley (1967) state that these compounds may adhere to the crucible wall and hinder further reaction or may be detached because of large differences in specific volume between compounds and base refractory and agitation within the melt. An example of this is HfO_2 which is more stable than Al_2O_3 or ZrO_2; a free energy of formation chart (Figure 2)

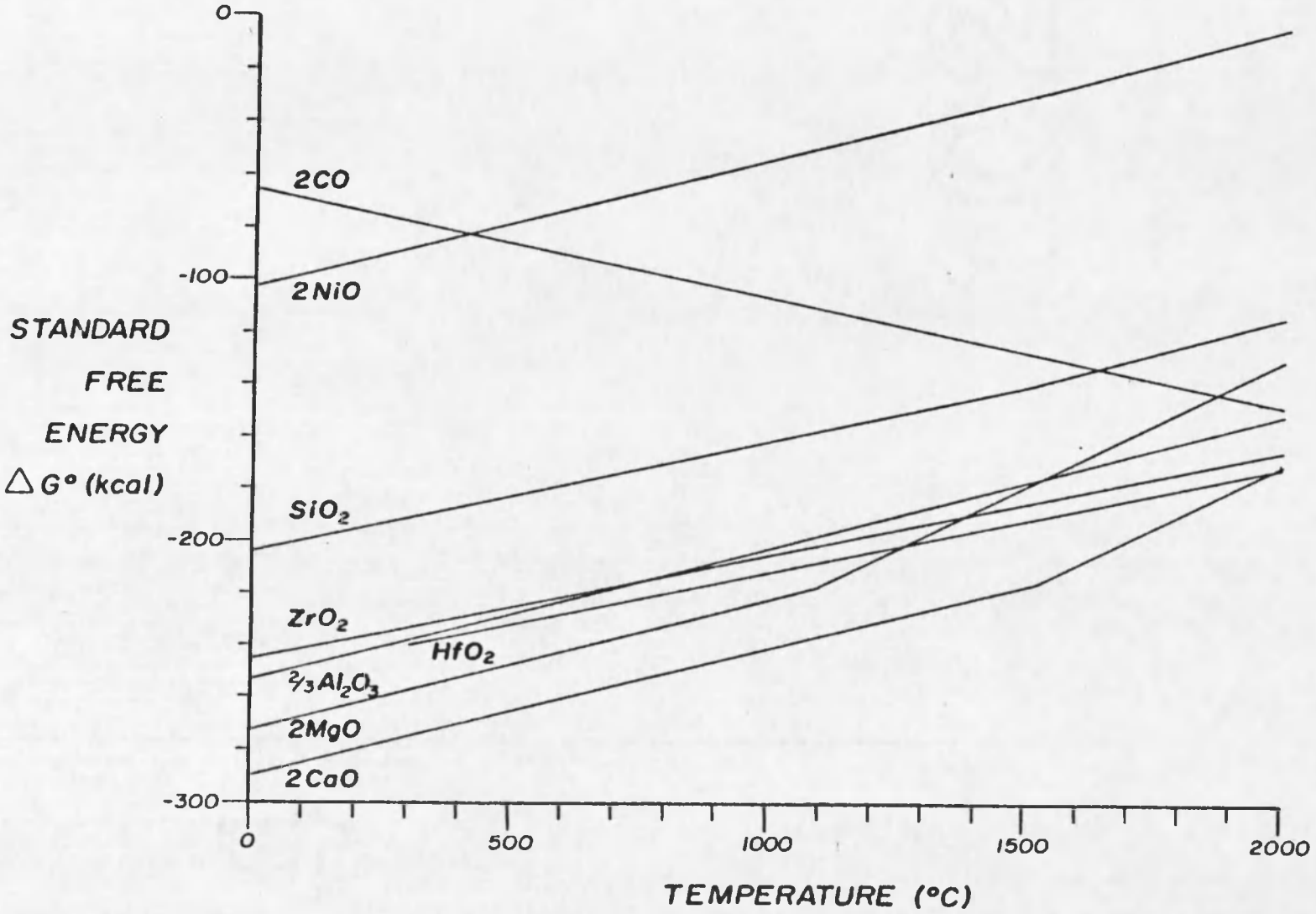

Fig. 2. Free energy of formation of oxides from their elements, per mole of O_2 (Cremisio, 1972; Sutton and Maurer, 1979).

is available for comparison. Thus, from thermodynamic considerations, HfO_2 is expected to form preferentially on the crucible walls relative to the original crucible composition. However, the activities of the alloy elements in the melt are also factors which must be considered. Reactions (16) and (17) represent a possible HfO_2 layer formation:

$$3\underline{Hf} + 2Al_2O_3(s) = 3HfO_2(s) + 4\underline{Al} \quad (16)$$

$$\underline{Hf} + ZrO_2(s) = HfO_2(s) + \underline{Zr} \quad (17)$$

Since CaO is also a crucible material, $\underline{Ca}$ near the crucible-melt interface will react with HfO_2 and Al_2O_3 according to reactions (18) and (19).

$$\underline{Ca} + HfO_2(s) + \underline{O} = CaHfO_3(s) \quad (18)$$

$$x\underline{Ca} + Al_2O_3 + y\underline{O} = Ca_xAl_2O_{(y+3)} \quad (19)$$

These phases are expected to form on the crucible walls. Sutton and Maurer (1979) state that with increasing melt time there is a build-up of oxide particles within the pores of the crucibles (along with metal droplets) and at the surface of the crucible. At the surface, oxide particles form and are apparently connected together to form a network which retains the metal (skull) within the interstices of the network, itself, after the melt has been poured. The metal in future melts actually "sees this type of a skull layer." Since the oxides in this type of skull layer are more chemically stable than the original crucible material, the rate of crucible decomposition is expected to

decrease with subsequent melts. This oxide layer could effectively act as a boundary between the liquid metal and the original crucible surface and hinder further reactions. This process is known as "conditioning" the crucible.

2.4 Reactions Within the Melt and at the Melt-Vacuum Interface

Inclusions form within the melt from various sources. Dissolved oxygen within the melt reacts with aluminum and hafnium to form oxide inclusions; from Figure 2 and Table 2, it is evident that the formations of Al_2O_3 and HfO_2 are thermodynamically very favorable.

$$2\underline{Al} + 3\underline{O} = Al_2O_3(s) \tag{20}$$

$$\underline{Hf} + 2\underline{O} = HfO_2(s) \tag{21}$$

The major sources of the oxygen in the melt are oxygen from the decomposing crucibles and oxygen within the chamber environment above the melt.

Since HfO_2 is more stable than the other oxides, HfO_2 inclusions also form at the expense of these oxides. An example of such a reaction which could occur within the melt is:

$$2Al_2O_3(s) + 3\underline{Hf} = 3HfO_2(s) + 4\underline{Al} \tag{16}$$

Carbon is used as a deoxidizer in nickel-base melts. The oxygen which reacts with carbon leaves the system as CO(g) instead of reacting with Al_2O_3 or HfO_2 to form inclusions. As the metal melts, a carbon boil

reaction takes place as carbon and oxygen combine, and CO(g) is continuously pumped out of the molten metal according to the reaction:

$$\underline{C} + \underline{O} = CO(g) \qquad (6)$$

This reaction is favored when the total pressure is decreased and temperature is increased. This carbon boil reaction decreases the amount of oxygen available to react with elements such as aluminum and hafnium to form inclusions. However, oxygen levels seldom reach those predicted by thermodynamic theory for the carbon-oxygen reaction because the rate at which oxygen enters the melt from the decomposition of the refractory eventually reaches the rate at which oxygen leaves the melt.

Cremisio (1972) states that the dissolution of refractories and/or the inability of critically sized Ca(g) bubbles to nucleate (due to the metallostatic head) are probably the major reasons for not achieving the theoretical levels of approximately 6-10 ppm. However, proper choice of crucibles, effective stirring, good control of vacuum and correct use and charging of raw materials all help in keeping oxygen levels consistently to approximately 20-30 ppm.

Other refractory dissociation products within the melt (Al, Hf, Zr, Ca, and Si) react with dissolved oxygen to form oxides. Again, these all float to the top to form a dross layer except HfO_2 which sinks to the bottom because of its high density. Magnesium in the melt has a high vapor pressure and is pumped out by the vacuum pump (similar to carbon monoxide) instead of reacting with oxygen to reform MgO inclusions.

CHAPTER 3

EXPERIMENTAL PROCEDURE

3.1 Experimental Apparatus

The melts were made in crucibles which were placed inside the induction coils of a Stokes Vacuum Casting (vacuum chamber) unit. Power was supplied to the induction coils by a 15 kilowatt Inductotherm generator. The temperature of the melt was measured by an optical pyrometer, and the pressure of the vacuum chamber was monitored by a vacuum ionization gage.

The crucible induction coil assembly is detailed in Figure 3. The crucibles were centered inside the induction coils by packing a fine alumina insulating powder as back-up material around the crucible; flexible asbestos sheet was used to contain the alumina powder along the sides of the induction coils. Around the top of the crucible assembly, magnesia powder, mixed with sodium silicate ("waterglass"), was used as a collar material to prevent the fine alumina powder from falling out when the crucible assembly was tipped to the pouring position. The outside support of the induction coils, as well as the top cover plate and the bottom support were constructed of transite.

A photograph of the crucible assembly within the vacuum chamber is shown in Figure 4; the control panel of the 15 kilowatt generator as well as the ionization gage is shown in Figure 5.

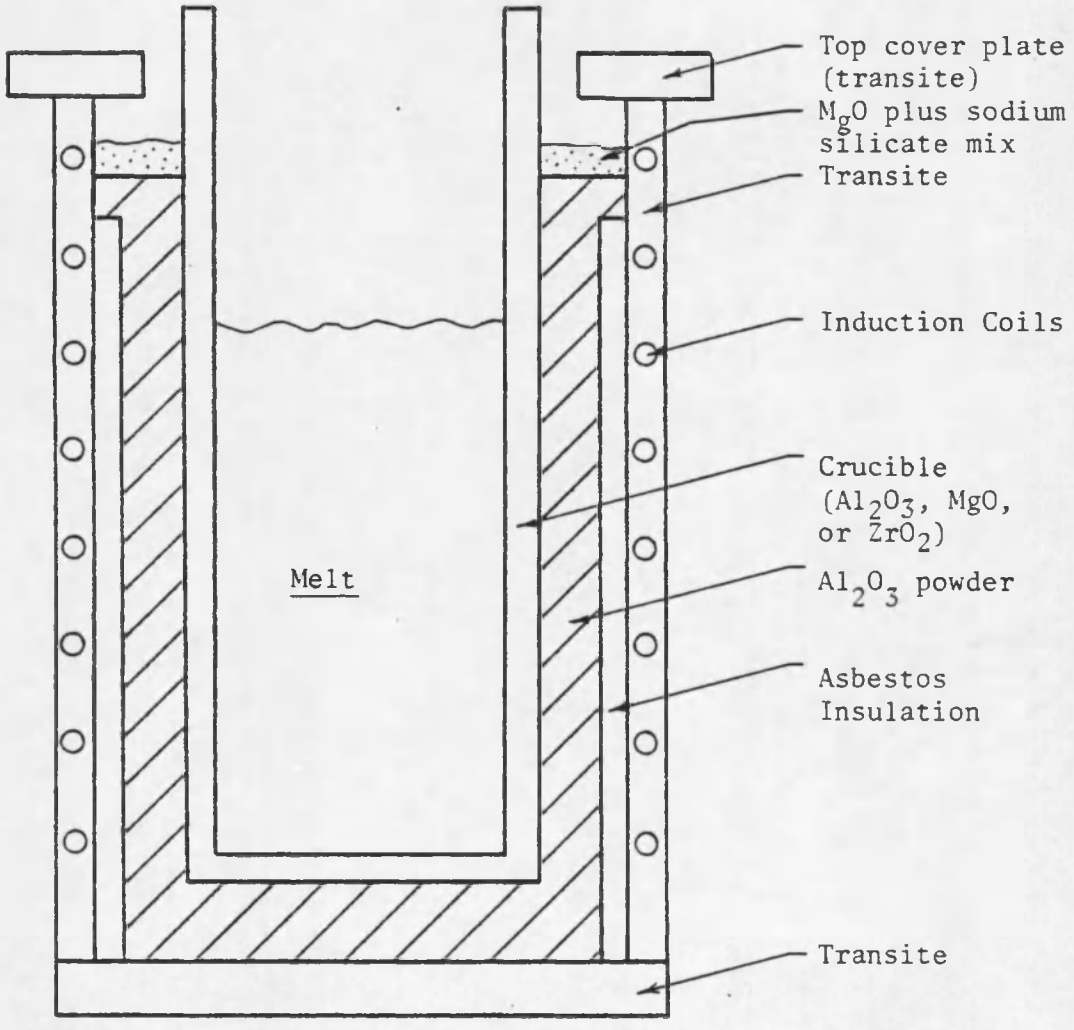

Fig. 3. Crucible assembly.

Fig. 4. Stokes vacuum casting unit.

Fig. 5. Generator control panel and vacuum ionization gage.

The liquid metal was poured into a sand mold prepared from silica mulled with sodium silicate and allowed to harden in air. An open top mold cavity was made using a wood pattern in the shape of an inverted bowl; the mold is sketched in Figure 6. This mold was set inside the vacuum chamber at the proper position so it could receive the liquid metal from the crucible during the pouring operation.

3.2 Melt Schedule

A series of 12 nickel-base vacuum melts was melted and cast. Before any experimental melts were made in a crucible, a "wash" heat was made. Pure nickel was heated to 1550°C under vacuum pressures (1-10 microns) and poured into ingots. This served to degas the crucibles. Four alloy compositions were used; these were Ni-0.15C, Ni-0.15C-5Al, Ni-0.15C-1Hf, and Ni-0.15C-5Al-1Hf. They were melted in three different crucibles; these were Al_2O_3, MgO, and ZrO_2 crucibles. The sequence of melts is shown in Table 4.

The alloy composition and the crucible type were the only two intended variables for these experiments. However, the pressure in Melts No. 11 and 12 was approximately 1 torr (1000 microns) because of problems with the mechanical pump; the pouring pressure in Melt 5 was an unexpected 200 microns. The other nine melts were melted under 1-10 microns pressure which is typical of industrial melting practice.

A temperature of 1550°C was selected as the temperature to which the alloy would be heated and poured. Since nickel melts at 1454°C, one hundred (100°C) degrees of superheat was used for all melts which is also typical of industrial practice.

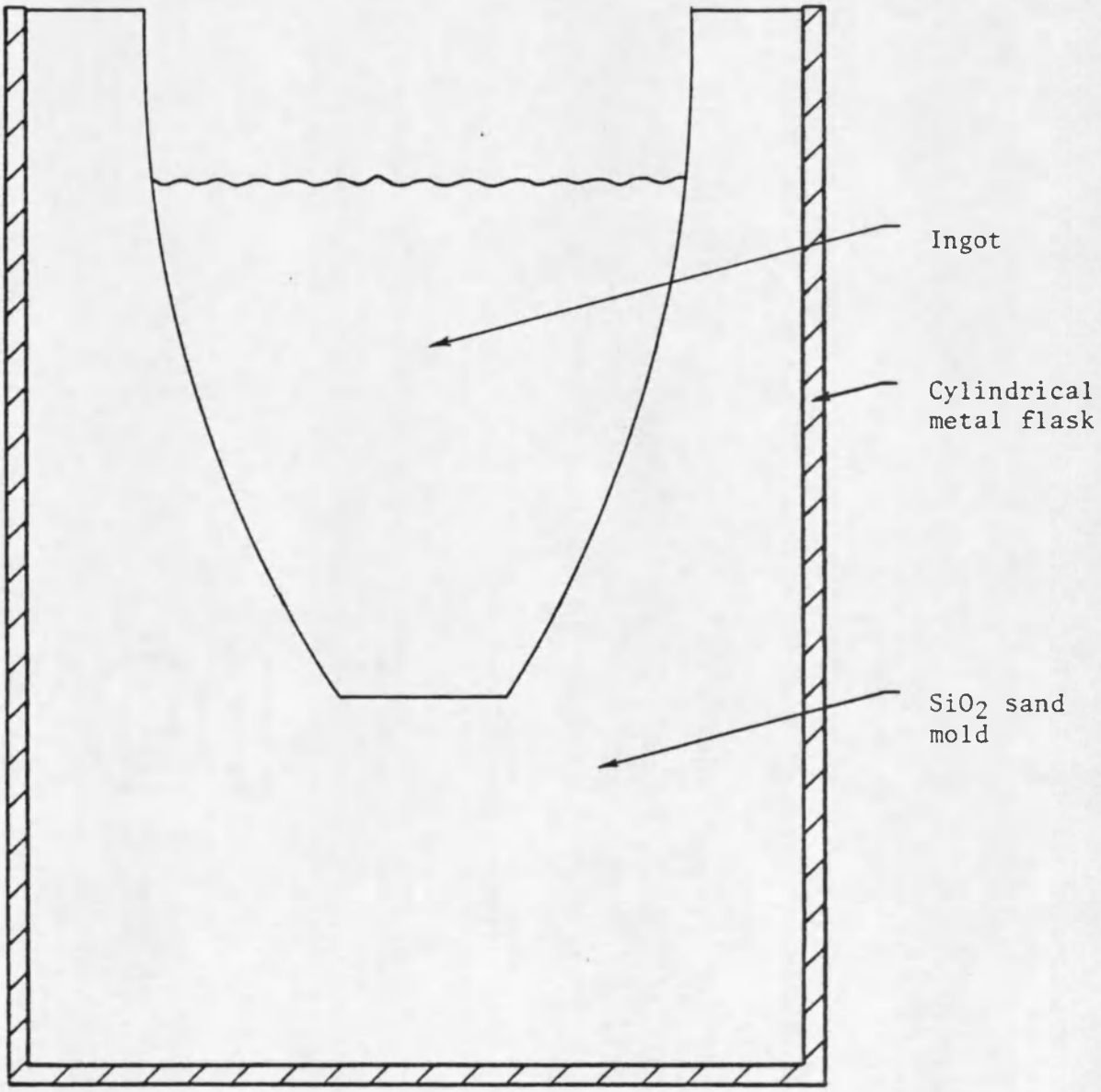

Fig. 6. Sketch of mold.

Table 4. Melt schedule.

Melt No.	Alloy	Crucible	Condition
1	Ni-0.15C	Al_2O_3	New (after wash heat)
2	Ni-0.15C-5Al	Al_2O_3	2nd heat
3	Ni-0.15C-1Hf	Al_2O_3	3rd heat
4	Ni-0.15C-5Al-1Hf	Al_2O_3	4th heat
5	Ni-0.15C	MgO	New (after wash heat)
6	Ni-0.15C-5Al	MgO	2nd heat
7	Ni-0.15C-1Hf	MgO	3rd heat
8	Ni-0.15C-5Al-1Hf	MgO	4th heat
9	Ni-0.15C	ZrO_2	New (after wash heat)
10	Ni-0.15C-5Al	ZrO_2	2nd heat
11	Ni-0.15C-1Hf	ZrO_2	3rd heat
12	Ni-0.15C-5Al-1Hf	ZrO_2	4th heat

The crucibles used in these melts were obtained from Norton; the composition and porosity of each of these crucibles are given in Table 5 (as supplied by the manufacturer). These crucibles are shown in Figure 7; the crucibles were 6 inches (15.2 cm) in height with an inside diameter of 2 3/4 inches (6.7 cm) and a wall thickness of 5/16 inches (0.8 cm).

For the melts, electrolytic nickel, remelted and cast into 1 cm diameter (approx.) spheres, and commercially pure aluminum were used. The hafnium contained significant amounts of Zr and Fe and was in strip form approximately 0.8 cm thick. The carbon was spectroscopically pure and in the form of graphite rods. The chemical compositions of the charge materials are given in Table 6.

3.3 Typical Melt Cycle

For each melt, the charge materials were carefully weighed. The nickel was in the form of small spherical pellets while the aluminum was in small chunks of about 10 grams. When hafnium was used, it was added as two small pieces of strip of about 8 grams each. The graphite rods were crushed with a mortar and pestle into a fine carbon powder. About 1400 grams of charge was used for each melt.

The nickel, aluminum, and hafnium were degreased with trichloroethylene, rinsed in distilled water, and then dryed at 140°C for 30 minutes. The metal was then charged into the crucible with the carbon powder sprinkled throughout the charge.

The crucible assembly was then placed inside the vacuum chamber and connected to the power leads. After closing the door, the chamber was pumped down with a mechanical pump to approximately 0.5 torr and then

Table 5. Chemical analysis of the crucibles.

Al_2O_3 Crucible (Porosity = 21%)	
Al_2O_3	99.01 wt. %
SiO_2	0.58 wt. %
Fe_2O_3	0.11 wt. %
Na_2O	0.17 wt. %
MgO Crucible (Porosity = 22%)	
MgO	99.00 wt. %
CaO	0.10 wt. %
SiO_2	0.50 wt. %
Al_2O_3	0.35 wt. %
Fe_2O_3	0.10 wt. %
ZrO_2 Crucible (Porosity = 25%)	
ZrO_2	92.00 wt. %
CaO	4.5 wt. %
HfO_2	1.5 wt. %
SiO_2	0.9 wt. %
Al_2O_3	0.6 wt. %
TiO_2	0.3 wt. %
Fe_2O_3	0.2 wt. %

Fig. 7. The MgO, Al_2O_3, and ZrO_2 crucibles.

Table 6. Chemical compositions of charge materials.

Nickel	
Ni	99.988 wt. %
C	0.002 wt. %
Co	0.010 wt. %
Aluminum	
Al	99.79 wt. %
C	0.01 wt. %
Fe	0.15 wt. %
Si	0.05 wt. %
Hafnium	
Hf	Balance
Fe	1.02 wt. %
Zr	3.8 wt. %
C	30 ppm
O	1620 ppm
Al	170 ppm
U	4.1 ppm

pumped down to the range of 1-10 microns pressure with a diffusion pump. When the lowest pressure was achieved the metal charge was heated and melted; during this period, the temperature was measured with an optical pyrometer approximately every two minutes. The pressure was also monitored and recorded every minute or two. The melt was heated to approximately 1550°C, held for about two minutes, and then poured into the silica sand mold to form an ingot. This melting sequence, starting with generator power turned on, usually took 15-20 minutes. The pressure in the chamber was kept low by the vacuum pumps for two more hours before bleeding in air to return the system to atmospheric pressure. This was done to minimize the oxidation of the ingots at the high temperatures. The ingots were then removed from the sand molds for subsequent operations. A typical ingot sectioned in two (top portion cut off on left side) is shown in Figure 8.

3.4 Metallography

Metallographic preparation was performed so that the ingots and the crucibles could be analyzed by optical microscopy and by microprobe analyses.

The ingots were sectioned into many pieces with an abrasive type cut-off wheel flooded with water for cooling. Specimens from the top and bottom surfaces were cut from the ingots and mounted in bakelite. Grinding and polishing were accomplished by first grinding successively on 240, 320, 400, and 600 grit papers and then polishing with diamond pastes on a very low nap nylon cloth (as recommended by Buehler Metallographic Supply Co. for polishing with the idea of retaining

Fig. 8. Typical ingot (sectioned in half).

inclusions). The two diamond pastes had particle sizes of 1 micron and 0.25 microns for coarse and fine polish, respectively. Kerosene was used as a lubricant during the polishing operation.

The crucibles were cut with a diamond cut-off wheel into sections small enough for 1 inch diameter mounts of epoxy. Two samples from each crucible were mounted; a top view of the bottom surface and a cross sectional view of the bottom surface of each crucible were mounted. The edge views of these sections are shown in Figure 9.

To prepare the epoxy mounts, the samples of the crucibles were heated on a hot plate to approximately 100°C. A 50-50 mixture of epoxy resin and hardener was applied to the crucible surface to be examined. These pieces were set on a piece of aluminum foil which had been sprayed with mold release; the aluminum foil was set on a very smooth, flat board. A one inch tubular mold was set around this sample, and then more epoxy was added until it completely submerged the sample and filled the mold. This was allowed to set overnight, and then it was cured at 60°C for 4 hours. These crucible mounts were then ground with 400 and 600 grit papers followed by the same polishing operation that was performed on the specimens of ingot material.

3.5 Optical Microscopy and Microprobe Analysis

The ingots were examined under a Versamet Unitron 5096 metallograph for evidence of inclusions throughout the solid ingot and oxide skins (dross) on the top and bottom surfaces of these same ingots. The crucible surfaces and "skull" material which adhered to the crucibles were also examined. Areas of interest were marked with either two or

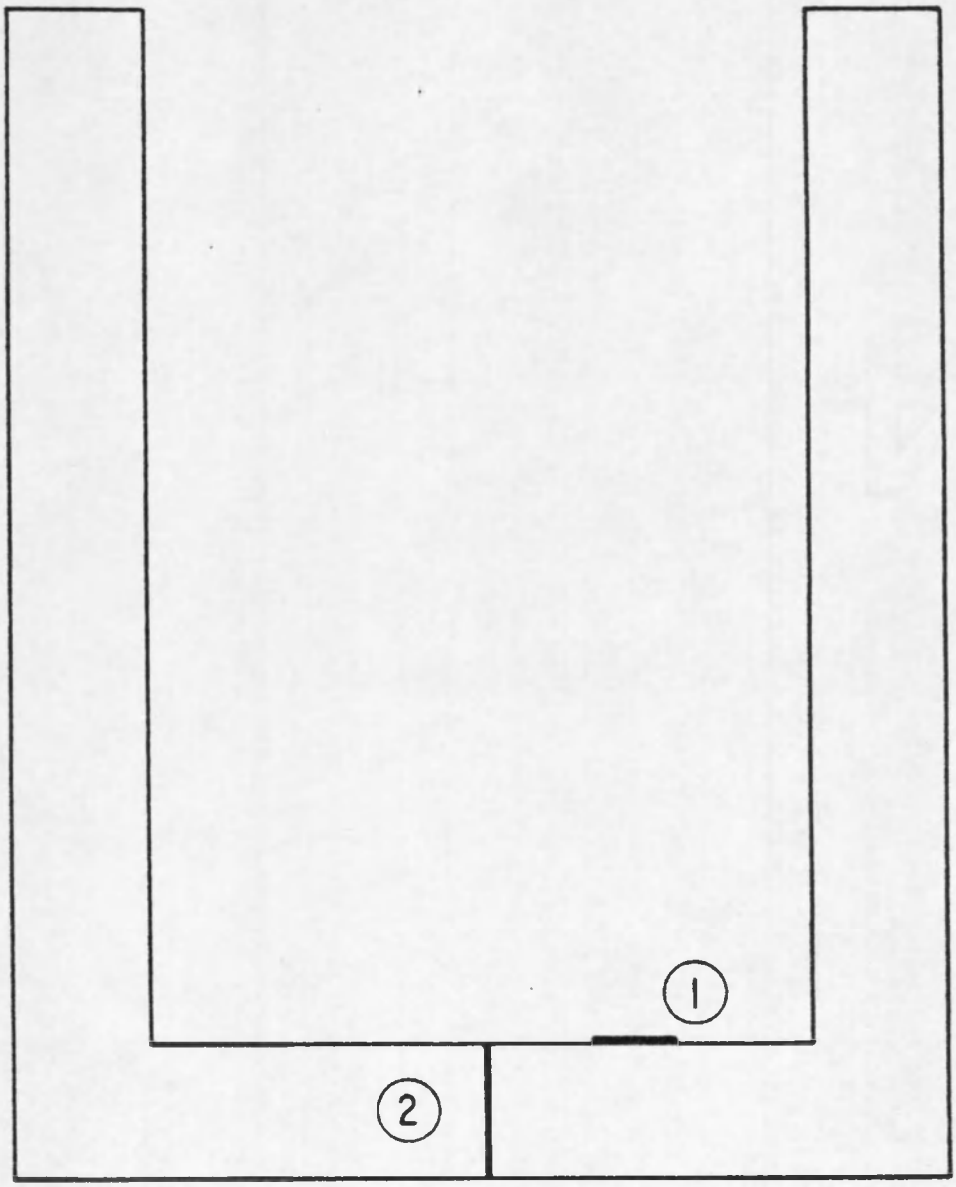

Fig. 9. Edge view of crucible sections.

1. Top surface of bottom of crucible.
2. Cross section of bottom of crucible.

three Vickers hardness indentations and then photographed on the metallograph. This was done as a convenience to locate these areas of interest in the microprobe unit.

The microprobe, or Scanning Electron Microprobe Quantometer (SEMQ), was used to obtain the chemical composition of samples. The wavelength dispersion method was employed in these chemical analyses. The microprobe used x-ray spectrometers to identify, and count x-rays based on their wavelength. The results were presented in two different manners. A numerical computer printout of the chemical composition of a probed region down to a size of 1 micron in diameter was obtained. The numerical value reported was the ratio of the x-ray intensity of each element in the specimen divided by the intensity of x-rays obtained from the pure standards; this ratio is often referred to as the "K-ratio." An oxide was used as the standard for oxygen.

Also, x-ray distribution images of certain key elements were obtained. These were very useful in determining the composition of various phases which appeared on the photomicrographs. Secondary electron pictures were also taken; these identify the exact location in which the composition data were obtained.

CHAPTER 4

RESULTS AND DISCUSSION

4.1 General Outline of Presentation

Twelve nickel-base heats were induction melted under vacuum and then cast into small open-top ingot molds. During the melting and pouring of the ingots, observations on the presence or absence of a surface scum or dross (i.e., oxides) were noted. These ingots were subsequently sectioned for metallographic and microprobe analyses. The results are discussed in terms of four different series of alloys. Ingots 1, 5, and 9 were analyzed together because these contain Ni-0.15C. Similarly, series of alloys containing Ni-0.15C-5Al (Ingots 2, 6, and 10), Ni-0.15C-1Hf (Ingots 3, 7, and 11), and Ni-0.15C-5Al-1Hf (Ingots 4, 8, and 12), respectively, are analyzed. In addition, samples removed from the melting crucibles were analyzed using the microprobe with emphasis on reaction products found on or near the melt surface of the crucibles after they had been used for four heats. Based upon these observations, a discussion of the inclusion or dross-forming reactions is presented.

4.2 Observations of Experimental Melts

The twelve nickel-base melts made in this study are shown in Table 5. The general plan was to melt and superheat the charge materials to 1550°C while under a vacuum of 1-10 microns, then to pour into sand molds to form the ingots. Nine melts, in fact, were prepared in this

manner, but the last two heats (11 and 12) were melted and poured under a vacuum of approximately 1 torr due to problems with the mechanical pump. The chamber pressure unexpectedly rose to 200 microns in Melt 5. This was probably due to incomplete outgassing in the wash heat. Complete details are shown in Table 7.

The logs of the twelve melts are recorded in Appendix A; the logs include chamber pressure, melt temperature, and observations of melting and formation of surface scum and the time of pour. For example, in the aluminum-bearing melts, a heavy dross layer or scum was noticed on the melt surface and on the top surface of the solidifying ingot. This dross layer formed during the later stages of the melting process. Figure 10 shows an example of the dross which formed on top of the solidified ingot. A carbon boil reaction was noticed in the early stages of all melts; during the boil, the melt surface was free of dross.

Melt 6 was allowed to stay molten for 31 minutes (see Table 7) in order to observe whether dross rose to the top surface when the power was turned off (no induction stirring). It was observed that dross rose to the top surface and collected near the crucible wall.

4.3 The Ni-0.15C Melts

Melts 1, 5, and 9 contained Ni-0.15C and were melted in Al_2O_3, MgO and ZrO_2 crucibles, respectively. For these melts, the crucibles were newly installed. In Ingot 9, grains of ZrO_2 from the melting crucible were found on the top surface. The x-ray distribution images of Ni and Zr on the top surface of this ingot are shown in Figure 11. In these images, the presence of white dots indicates the presence of the given

Table 7. Melt data.

Melt No.	Alloy	Crucible	Crucible Condition	Pressure at Meltdown (Microns)	Time Maintained Molten (Minutes)	Pressure at Pour (Microns)
1	Ni-0.15C	Al_2O_3	New	7	4	12
2	Ni-0.15C-5Al	Al_2O_3	2nd heat	6	5	9
3	Ni-0.15C-1Hf	Al_2O_3	3rd heat	4	5	7
4	Ni-0.15C-5Al-1Hf	Al_2O_3	4th heat	4	4	5
5	Ni-0.15C	MgO	New	60	4	200
6	Ni-0.15C-5Al	MgO	2nd heat	4	31	12
7	Ni-0.15C-1Hf	MgO	3rd heat	4	6	8
8	Ni-0.15C-5Al-1Hf	MgO	4th heat	4	5	4
9	Ni-0.15C	ZrO_2	New	4	4	5
10	Ni-0.15C-5Al	ZrO_2	2nd heat	2	4	4
11	Ni-0.15C-1Hf	ZrO_2	3rd heat	1400	5	1200
12	Ni-0.15C-5Al-1Hf	ZrO_2	4th heat	1200	8	> 2000

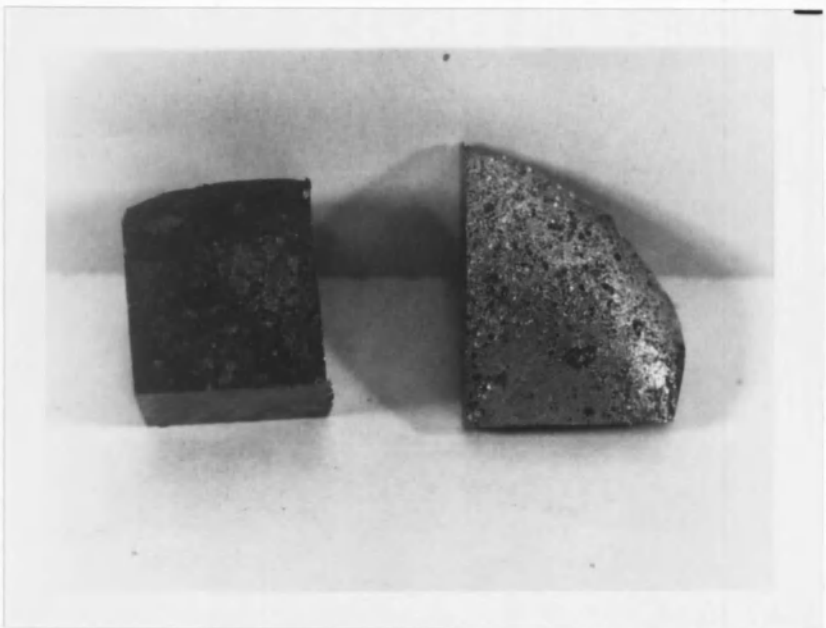

Fig. 10. Typical top surfaces of ingots.

Notice the dross layer present on the top surface.

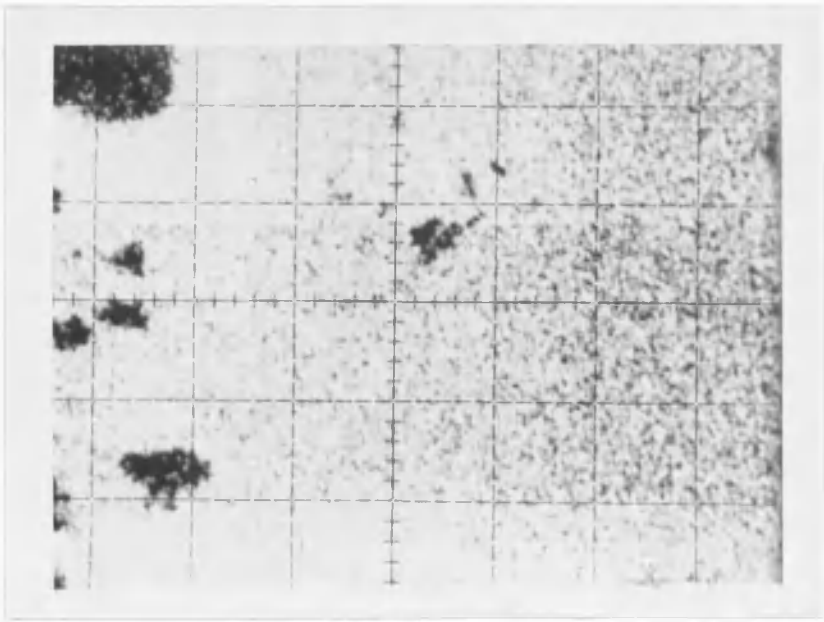

(a)

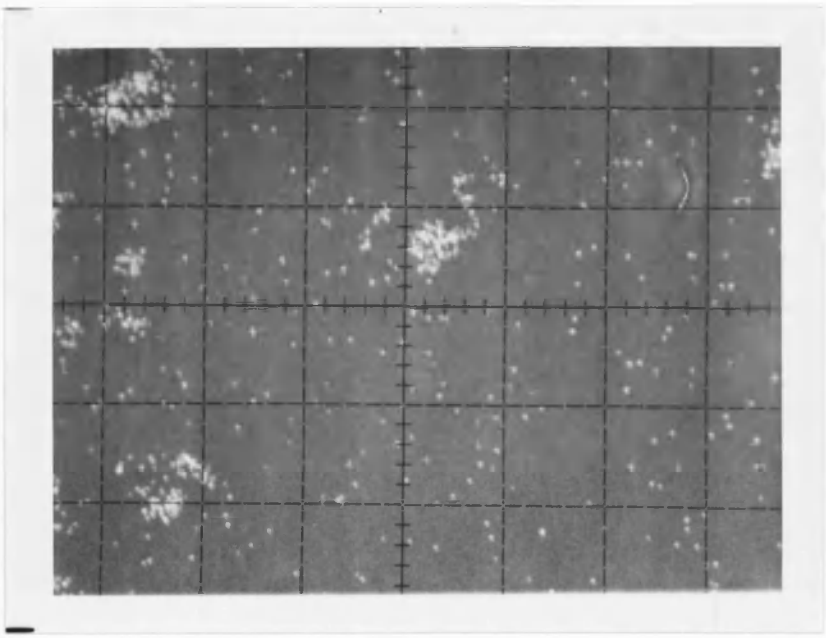

(b)

Fig. 11. Distribution of nickel and zirconium on the top surface of Ingot 9.

(a) Nickel image.
(b) Zirconium image. The concentration of white dots is roughly proportional to the concentration of the respective element. The upper left hand corner contains appreciable amounts of SiO_2. Magnification is 200x.

element. Conversely the dark areas represent an absence of the given element. To complement the images of Figure 11, the microprobe beam was fixed on a nickel rich area (metallic matrix) and on a zirconium rich area (oxide matrix), respectively. Table 8 gives the K-ratios found in these two areas. The K-ratio is the intensity ratio defined as the X-ray intensity of the element in the matrix divided by the intensity of that element in its pure form; an oxide is used as a standard for oxygen. The metallic matrix appears to be relatively pure Ni, but it should be noted that the microprobe used does not detect carbon at the composition of the alloys studied. The reported K-ratios for the nickel was greater than one. The fact that K-ratios were greater than one throughout this study suggests that the probe was not properly calibrated. However, since only a semi-quantitative analysis is performed, the meaning of the results is not affected. In the oxide matrix, the intensity ratios for zirconium and oxygen are very high which suggests that these Zr-rich regions are ZrO_2 grains. Calcium, silicon, and hafnium are reported because the ZrO_2 crucible contains 4-5% CaO, 0.9% SiO_2 and 1.5% HfO_2; the crucible was the only source of zirconium, calcium and hafnium in the system. In fact, the region in the upper left hand corner of Figure 11 is rich in SiO_2. Therefore, it appears that grains of ZrO_2 have eroded or fallen from the crucible into the melt.

No appreciable amounts (> 0.001) of any element other than nickel (carbon not reported) was found on the top surfaces of Ingots 1 and 5. This suggests that no significant oxide phase forms on the top surfaces of these melts; this agrees with visual observations. Thus, no

Table 8. Microprobe analysis of dross of Ingot 9.

	K-ratios	
	Metallic Matrix	ZrO_2 Grains
Ni	> 1.0	0.020
Hf	< 0.001	0.004
Ca	0.001	0.094
Si	0.001	0.22
Zr	< 0.001	0.30
O	0.004	0.50

Al_2O_3 or MgO crucible decomposition is evident from the results of the examinations of the top surface of these melts with Ni-0.15C.

In this series of melts, the most significant finding was that some ZrO_2 grains have eroded from the crucible. However, no Al_2O_3 or MgO crucible decomposition is evident by analyzing these Ni-0.15C melts.

4.4 The Ni-0.15C-5Al Melts

Three Ni-0.15C-5Al melts (Melts 2, 6, and 10) were cast in this study. The major finding of the probe results was that the inclusions on the top surfaces of all three ingots were rich in aluminum (presumably as Al_2O_3 and/or alumino-silicates). In these drosses relatively large concentrations of silicon were usually present. It also appears that the MgO crucible decomposed as is evident from the K-ratios of Mg and Ca given in Table 9 for Ingot 6. More evidence of ZrO_2 crucible erosion was noticed in that ZrO_2 grains were found on the top surface of Ingot 10;

Table 9. Microprobe analyses of dross areas on Ingot 6.

	K-Ratios		
	Al_2O_3-rich area	MgO-rich area	Metallic matrix (Ingot 2)
Ni	0.040	0.014	> 1.0
Al	0.83	0.35	0.016
Ca	0.24	0.036	0.000
Mg	0.20	0.27	0.000
Si	0.19	0.017	0.001
O	0.59	> 1.0	0.004

these grains were coated with a nonmetallic phase rich in aluminum, silicon, and oxygen (probably mullite).

Evidence for the foregoing results is given in Figures 12-17 and Tables 9-12. Figures 12 and 13 are a photomicrograph and a back-scattered electron image, respectively, of oxides (dross) found on the top surface of Ingot 6. Figures 14 and 15 show that there are significant concentrations of Al, Mg, and Si in this dross. The Al X-ray distribution image (Figure 14a) shows regions of heavy concentration of aluminum. It can be deduced that this Al-rich region does indeed contain Al_2O_3 from the equilibrium constant for Al_2O_3 in nickel melts at elevated temperatures (see Table 2). Using similar reasoning, the relatively rich concentrations of Mg and Si in Figures 14(b) and 15, respectively, are interpreted to be MgO and SiO_2. The obvious presence of Mg in Figure 14(b) is convincing evidence of MgO crucible decomposition. The MgO is

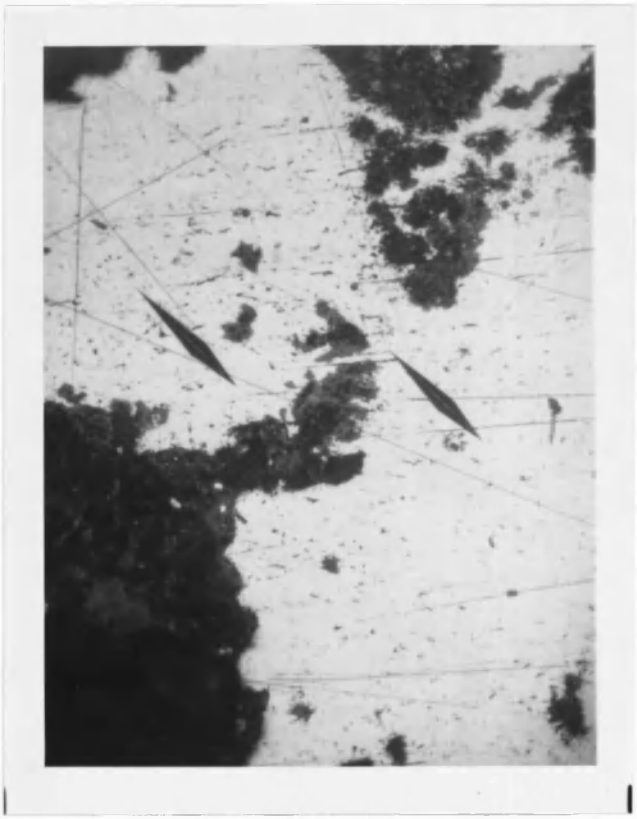

Fig. 12. Dross rich area on top of Ingot 6.

Magnification is 150x.

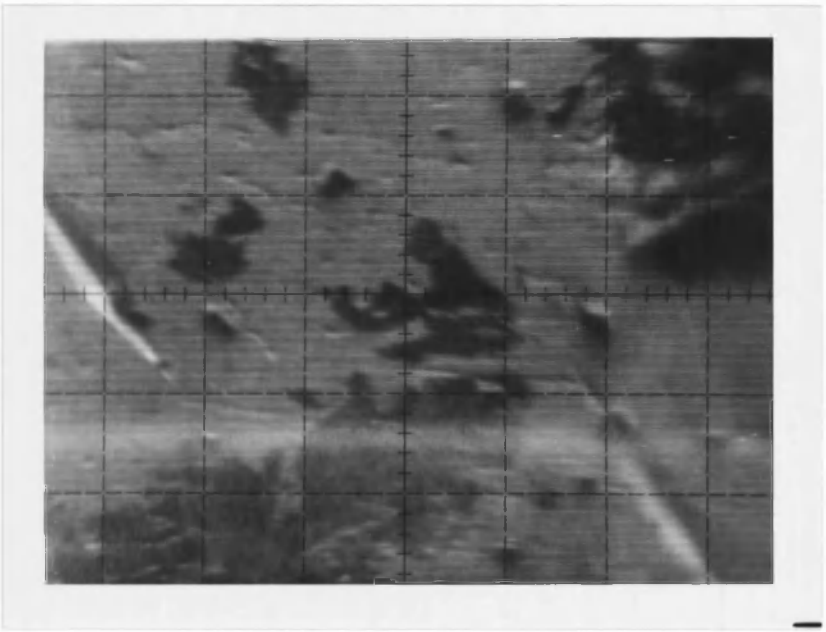

Fig. 13. Back-scattered electron image of area in Fig. 12. Magnification is 200x.

(a)

(b)

Fig. 14. Distribution of aluminum and magnesium on the top surface of Ingot 6.

(a) Aluminum distribution.
(b) Magnesium distribution. Notice that the Mg is always within an Al rich region. Magnification is 200x.

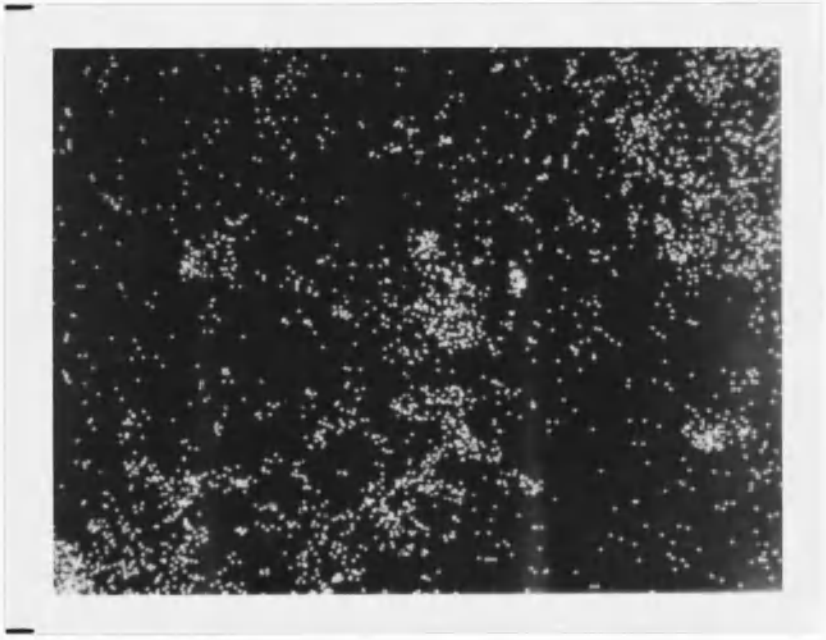

Fig. 15. Silicon x-ray distribution image of area in Fig. 14. White dots represent SiO_2. Magnification is 200x.

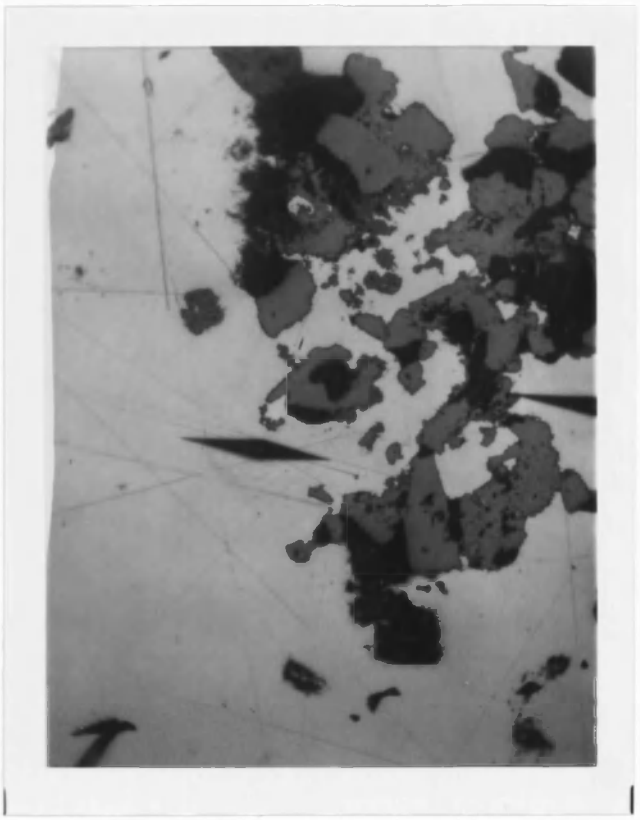

Fig. 16. ZrO_2 grains on the top surface of Ingot 10. Magnification is 150x.

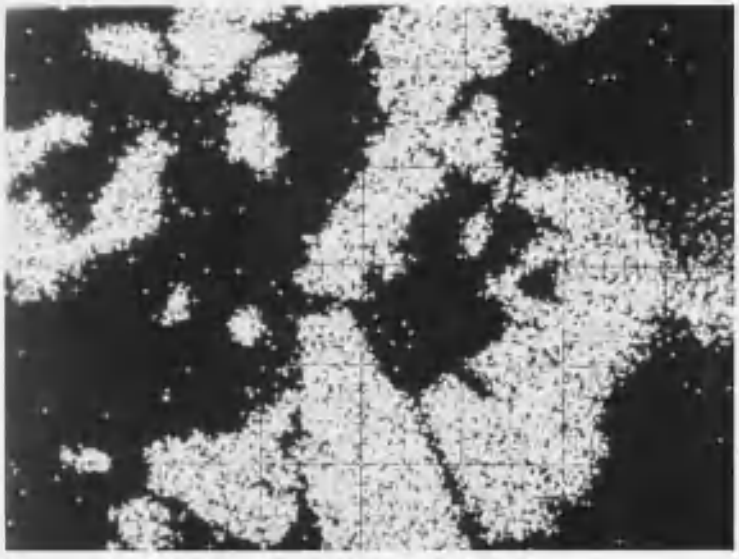

(a)

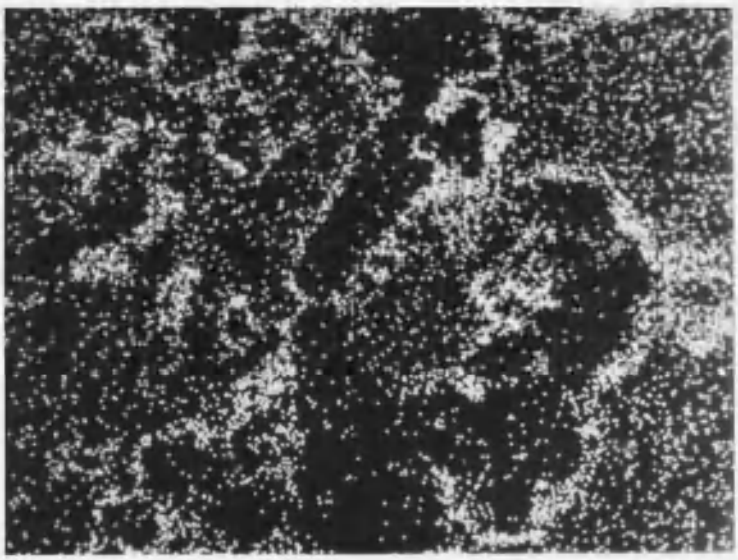

(b)

Fig. 17. Distribution of zirconium and aluminum on the top surface of Ingot 10.

(a) Zirconium distribution.
(b) Aluminum distribution. Notice that the Al_2O_3 coats the crumbs. Magnification is 200x.

Table 10. Microprobe analysis of top surface of Ingot 2.

	K-Ratios	
	Al_2O_3-rich area	Metallic matrix
Ni	0.18	> 1.0
Al	0.77	0.016
Si	0.29	0.001
O	0.33	0.004

Table 11. Microprobe analysis of a ZrO_2 grain on the top surface of Ingot 10.

	K-Ratios	
	ZrO_2-rich area	Metallic matrix
Ni	0.003	> 1.0
Al	0.002	0.027
Hf	0.017	0.000
Ca	0.24	0.000
Si	0.010	< 0.001
Zr	0.77	< 0.001
O	0.22	0.004

Table 12. Microprobe analysis of Al_2O_3-rich coating on a ZrO_2 grain on the top surface of Ingot 10.

	K-Ratios
	Al_2O_3-rich area
Ni	0.32
Al	0.16
Hf	0.001
Ca	0.011
Si	0.33
Zr	< 0.001
O	0.19

coincidental with Al_2O_3 probably as a result of combining with the Al_2O_3 to form a spinel ($MgAl_2O_4$) phase within the dross. Silica (SiO_2) is also noticed (Figure 15) in the aluminum rich areas. In fact, it was noticed in all three ingots that SiO_2 rich regions were always within Al_2O_3 rich regions; the SiO_2 was never separate from the Al_2O_3. Microprobe analyses of these various regions of Ingot 6 are shown in Table 9. The first analysis was performed in the Al-rich region in the upper right hand corner of Figure 14(a) while the second analysis was performed in the area richer in Mg near the bottom of Figure 14(b). The comparison of the oxygen K-ratios in these regions with the ratio in the metallic matrix shows that an oxide dross definitely formed. High aluminum contents (relative to the metallic matrix) are reported in this dross layer; this

is obvious evidence of Al_2O_3 rich dross on the top surface of the ingot. Notice that there appears to be more aluminum than any other element (except oxygen) in this dross. In this Al_2O_3 rich area, there are significant concentrations of Ca and Mg, and in the MgO rich area there is Mg and a lesser concentration of Ca. Therefore, the significant Mg and Ca compositions in this dross is clear evidence of MgO crucible decomposition. The Si K-ratios were also much higher in the dross than in the metallic matrix which indicates that the dross is partially comprised of SiO_2. This silicon can originate from any of three sources. Silicon is present in the original charge aluminum, the MgO crucible, and the sand mold. It is doubtful that the silicon in the dross is from sand grains of the mold because such grains would probably appear as relatively large chunks of virtually pure SiO_2 which is not evident in Figures 14 and 15. The silicon most likely originates from both the trace amounts in the original aluminum charge and from the MgO crucible. The appreciable concentration of calcium in the dross is further evidence of MgO crucible decomposition since the crucible, itself, is the only source of calcium. This is also consistent with the findings of Sutton and Maurer (1979) who predict that calcium aluminates form in aluminum-bearing nickel-base melts contained in MgO crucibles.

The top surface of Ingot 2 also had an Al_2O_3 rich dross layer with significant amounts of SiO_2 contained within. A microprobe analysis of the dross layer as compared with a metallic matrix sample of this ingot is shown in Table 10. Again, from the aluminum, silicon, and oxygen K-ratio data, it is evident that Al_2O_3 and SiO_2 are present on the surface

of Ingot 2. It can not be definitely determined whether the Al_2O_3 crucible decomposes because there is 5% Al in the alloy and small amounts of silicon in the aluminum charge metal.

The analysis of Ingot 10 once again shows clear evidence of ZrO_2 crucible erosion. Figure 16 shows grains of ZrO_2 on the top surface of the ingot. An x-ray distribution image of Zr (Figure 17a) clearly shows these grains are indeed rich in Zr. A microprobe analysis of a grain is shown in Table 11; the detection of an appreciable amount of Ca and lesser amounts of Hf and Si also suggests that these grains originated from the ZrO_2 crucible. It appears that the ZrO_2 grains crumbled as a whole without appreciably breaking up in the melt.

An interesting observation about the ZrO_2 grains is that an oxide layer rich in aluminum and silicon (Figure 17b and Table 12) coats the ZrO_2 grains. It is deduced that the ZrO_2 grains are partially reduced by the aluminum to form Al_2O_3 and elemental Zr which goes into the metallic solution. Alumina (Al_2O_3) is more stable than ZrO_2 in nickel-base melts as shown by the equilibrium constants in Table 2. Also, there is 5% Al and initially no Zr (initial activity of Zr = 0) in the melt; these factors favor the reduction of ZrO_2 by the aluminum. However, since the silicon K-ratio is so high, it is also possible that a silicate slag wets these ZrO_2 grains causing a silicate coating to form.

The analyses of the Ni-0.15C-5Al melts show considerable evidence of Al_2O_3 rich dross layers on the top surface of all three ingots. Clear evidence of MgO crucible decomposition was established by the fact that Mg, Ca, and Si were present in the dross on the top surface of Ingot 6. Again, it is noticed that ZrO_2 grains break off of the crucible as in

Ingot 10. A layer rich in Al_2O_3 and SiO_2 coated these ZrO_2 grains. No clear evidence of Al_2O_3 crucible decomposition could be established in Melt 2 since 5% Al which contains trace amounts of silicon is added to the melt.

4.5 The Ni-0.15C-1Hf Melts

The most significant finding from the probe results of the Ni-0.15C-1Hf melts is that appreciable amounts of HfO_2 dross form on the bottom surfaces of the three ingots. It is believed that silica (SiO_2) combines with the HfO_2 to form a $xHfO_2 \cdot ySiO_2$ phase in much the same manner as it combines with aluminum in the Ni-0.15C-5Al melts to form a mullite phase. Once again, considerable evidence of ZrO_2 crucible erosion was observed while only slight evidence of MgO crucible decomposition was noticed. On the ZrO_2 crucible grains, a HfO_2 coating very similar in nature to the Al_2O_3 coating on the ZrO_2 grains in the Ni-0.15C-5Al melts is present.

Hafnium oxide dross was found on the bottom surface of Ingot 3. A photomicrograph and a Hf x-ray distribution image of such a region are shown in Figures 18(a) and 18(b), respectively. A microprobe analysis of this dross region is compared with a metallic matrix region in Table 13. The relatively high Ni K-ratio in the HfO_2 dross region is probably due to the electrons from the beam striking the surrounding metallic matrix. The appreciable Si and Zr K-ratios in the HfO_2 dross is clear evidence of SiO_2 and ZrO_2 phases in the HfO_2 rich dross. It is theorized that the lighter SiO_2 and ZrO_2 particles agglomerate with the HfO_2 rich clusters and sink to the bottom of the melt with it. The source of this Zr

(a)

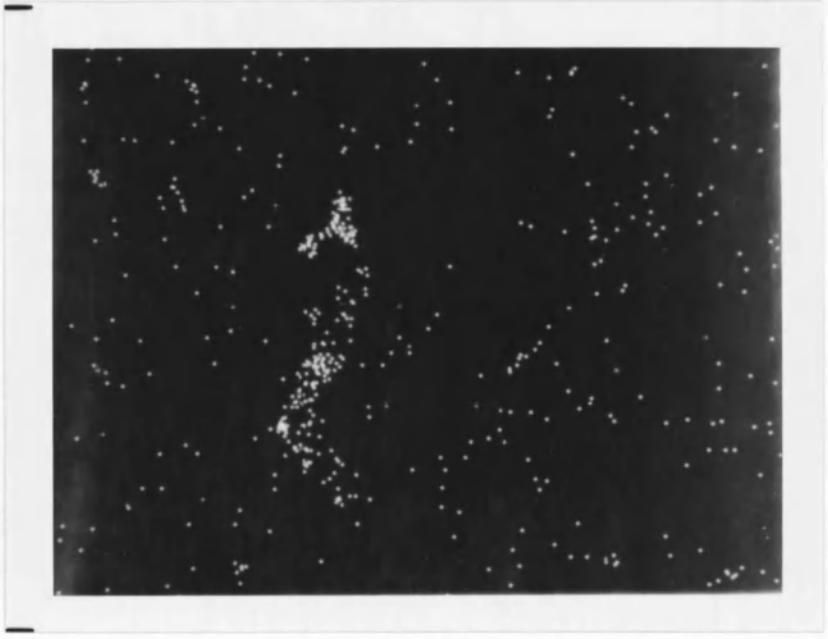

(b)

Fig. 18. HfO_2 dross on the bottom surface of Ingot 3.

(a) Photomicrograph.
(b) Hafnium x-ray distribution image. Magnification is 300x.

Table 13. Microprobe analysis of HfO_2 dross on Ingot 3.

	K-Ratios	
	HfO_2 Dross	Metallic Matrix
Ni	0.39	0.90
Al	0.009	0.004
Hf	0.56	0.008
Si	0.16	0.001
Zr	0.009	< 0.001
O	0.23	0.002

was the hafnium charge metal. It is believed that the Si originates from the retained nickel rich skull from the previous (Ni-0.15C-5Al) melt. The aluminum retained in this skull had trace amounts of silicon within it. This is discussed in more detail in section 4.7. Although no binary phase diagram data involving HfO_2 are apparently available, it appears that many different phases involving HfO_2, ZrO_2, and SiO_2 are present in this dross on the bottom surfaces of the ingots.

Microprobe analyses of Ingot 7 also show this HfO_2 rich dross on the bottom surface. A photomicrograph and a Hf x-ray distribution image of a dross region are shown in Figures 19(a) and 19(b). Microprobe analyses of the HfO_2 rich areas and the metallic matrix are shown in Table 14. Oxides from the decomposed MgO crucible tended to combine with the HfO_2 to form a dross consisting of many phases involving these compounds. This is evident by the appreciable Mg, Ca, and Si K-ratios in

(a)

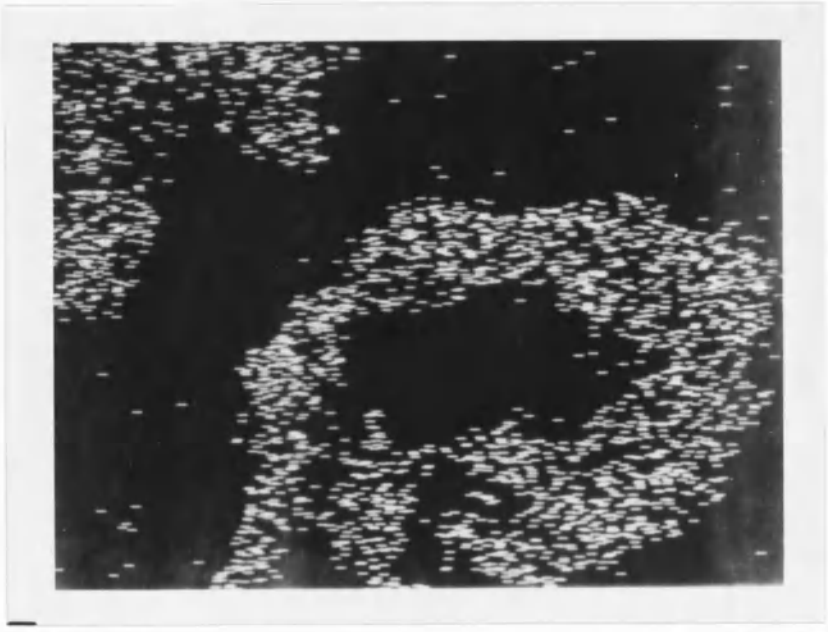

(b)

Fig. 19. HfO_2 dross on the bottom surface of Ingot 7.

(a) Photomicrograph.
(b) Hf x-ray distribution image. Magnifications are 150x and 200x for (a) and (b) respectively.

The large black area in (a) is believed to be a cavity.

Table 14. Microprobe analysis of HfO_2 on Ingot 7.

	K-Ratios		
	HfO_2-rich dross area no. 1	HfO_2-rich dross area no. 2	Metallic matrix
Ni	0.26	0.023	0.87
Al	< 0.001	0.001	0.003
Hf	0.34	0.73	0.006
Ca	0.000	0.011	0.005
Mg	0.006	0.009	0.001
Si	0.015	0.007	0.008
Zr	0.007	0.020	< 0.001
O	0.19	0.30	0.009

the dross. It should be noted that particles of $CaHfO_3$ ($CaO \cdot HfO_2$) were found by Sutton and Maurer (1979).

The bottom surface of Ingot 11 was also covered with this HfO_2 dross. A much larger portion of the bottom surface was covered with this dross which is expected since the vacuum pressure during melting was approximately 1 torr (1000 microns).

On the top surface of Ingot 11, ZrO_2 grains were again found. A comparison of the composition of these grains, the grains from Ingot 10, and a ZrO_2 crucible matrix sample is shown in Table 15. Since these compositions are nearly identical, it is theorized that the ZrO_2 grains erode and rise to the top of the melt without appreciable dissolution in the melt. In other words, the ZrO_2 rich areas on the top surface of the ingot are believed to be grains from the original ZrO_2 crucible as opposed to reaction products that form within the melt and float to the top.

Table 15. Microprobe analyses of ZrO_2 crucible grains.

	K-Ratios		
	Ingot No. 11	Ingot No. 10	ZrO_2 Crucible Matrix
Ni	0.002	0.003	< 0.001
Al	< 0.001	0.002	0.001
Hf	0.015	0.017	0.018
Ca	0.15	0.24	0.19
Si	0.002	0.010	0.000
Zr	0.65	0.77	0.79
O	0.29	0.22	0.29

Hafnium oxide coated the outside of these grains in much the same manner as the Al_2O_3 coated the outside of the grains in Ingot 10. It is believed that hafnium in the melt reduces the ZrO_2 crumbs just as aluminum did in Ingot 10. A microprobe analysis of this coating is shown in Table 16.

The major finding of the probe work on the Ni-0.15C-1Hf ingots is that HfO_2 rich dross defects form on the bottom surface of the three ingots. Zirconia (ZrO_2) crucible erosion was again found as well as MgO crucible decomposition. Again, no positive evidence of Al_2O_3 crucible decomposition could be established by analyzing these ingots; note the low Al K-ratios in all of these microprobe results.

Table 16. Microprobe analysis of HfO_2 coating on ZrO_2 grains on the top surface of Ingot 11.

	K-Ratios
	HfO_2 Coating
Ni	0.018
Al	0.002
Hf	0.24
Ca	0.016
Si	0.15
Zr	0.004
O	0.12

4.6 The Ni-0.15C-5Al-1Hf Melt

The probe results for this series of alloys could be described as the "summation" of the results of the three previous alloy series. Of course this is an oversimplification, but the results found in this series are strikingly similar to the combined results of the other three series of alloys. Again, alumina rich dross collected at the top of all three ingots while hafnium oxide rich dross covered the bottom of the three ingots. The ZrO_2 grains were evident in Ingot 12 while appreciable amounts of MgO crucible decomposition were noticed when analyzing Ingot 8. Alumina crucible decomposition again could not be established since 5% Al containing trace amounts of silicon was added to the melt.

Examples of the Al_2O_3 rich and HfO_2 rich dross on the top and bottom surfaces, respectively, of various ingots are shown in Tables 17 and 18. Notice that the ratio of aluminum to hafnium is much higher in

Table 17. Microprobe analysis of HfO_2 dross on bottom surface of Ingot 4.

	K-Ratios		
	Metallic Matrix	HfO_2-rich area no. 1	HfO_2-rich area no. 2
Ni	> 1.0	0.43	0.86
Al	0.028	0.14	0.048
Hf	0.003	0.24	0.17
Si	< 0.001	0.001	0.021
Zr	< 0.001	< 0.001	0.002
O	0.005	0.056	0.092

Table 18. Microprobe analysis of Al_2O_3 dross on top surface of Ingot 12.

	K-Ratios		
	Metallic Matrix	Al_2O_3-rich area no. 1	Al_2O_3-rich area no. 2
Ni	> 1.0	0.25	0.093
Al	0.030	0.23	0.78
Hf	0.002	0.12	0.14
Ca	< 0.001	0.011	0.002
Si	0.005	0.005	< 0.001
Zr	< 0.001	0.012	0.014
O	0.01062	0.56	0.42

the top surface dross on Ingot 12 than on the bottom surface dross on Ingot 4.

4.7 The Al_2O_3, MgO, and ZrO_2 Crucibles

Much information about the chemical reactions leading to the formation of inclusions and dross defects was learned by analyzing the crucible surfaces. Both top views and cross-sectional views of the bottom surface of the three crucibles (see Figure 9) were analyzed under the microprobe. The three crucibles were analyzed only after all four melts had been made.

The ZrO_2 crucible was coated with a layer of HfO_2; nickel base metal droplets were scattered throughout this layer. A back-scattered electron image of such a region is shown in Figure 20(a) while x-ray distribution images of zirconium, hafnium, and nickel are shown in Figures 20(b), 21(a), and 21(b), respectively. Comparisons of the chemical analyses of the interior of the ZrO_2 crucible, hafnium oxide coating, and nickel droplets are shown in Table 19. These x-ray distribution images and microprobe analyses definitely show that a HfO_2 coating formed on the ZrO_2 crucible. However, the melting pressure in the two hafnium-bearing melts in the ZrO_2 crucible was approximately 1-2 torr (1000-2000 microns). It is not known whether a much thinner HfO_2 coating would form if the melt had been made under the prescribed 1-10 microns. Sutton and Green (1977) reported that HfO_2 forms at the drop base during sessile drop studies of a hafnium-bearing nickel-base alloy on a ZrO_2 substrate. Also, Sutton and Maurer (1979) reported large quantities of HfO_2 in the skull of their ZrO_2-Prefire crucible. The nickel droplets probably formed

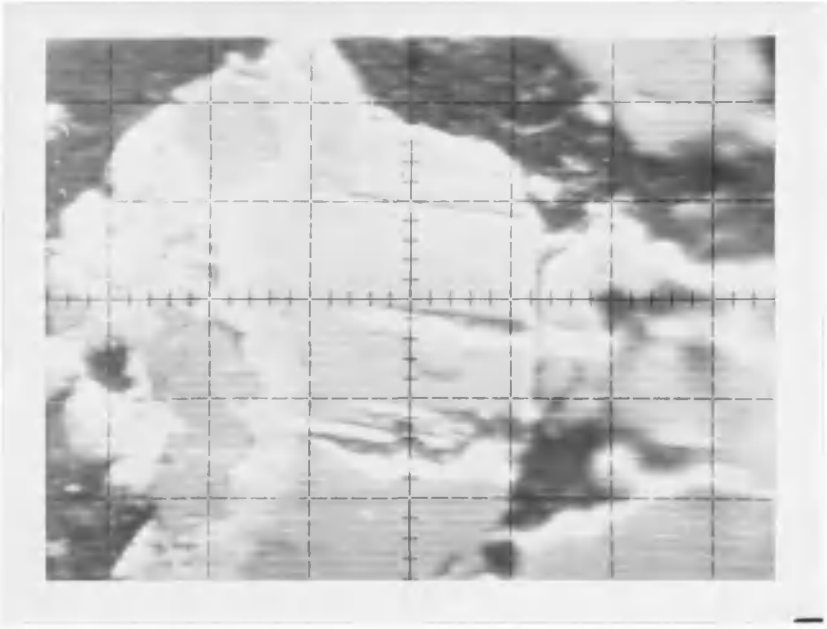

(a)

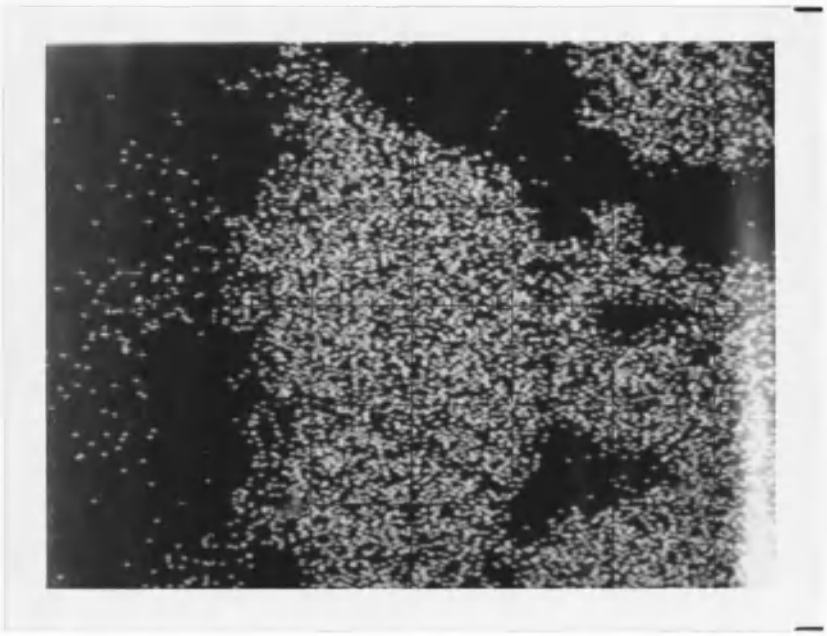

(b)

Fig. 20. Side view of ZrO_2 crucible sample.

(a) Back-scattered electron photograph.
(b) Zirconium x-ray distribution image.
Magnification is 200x.

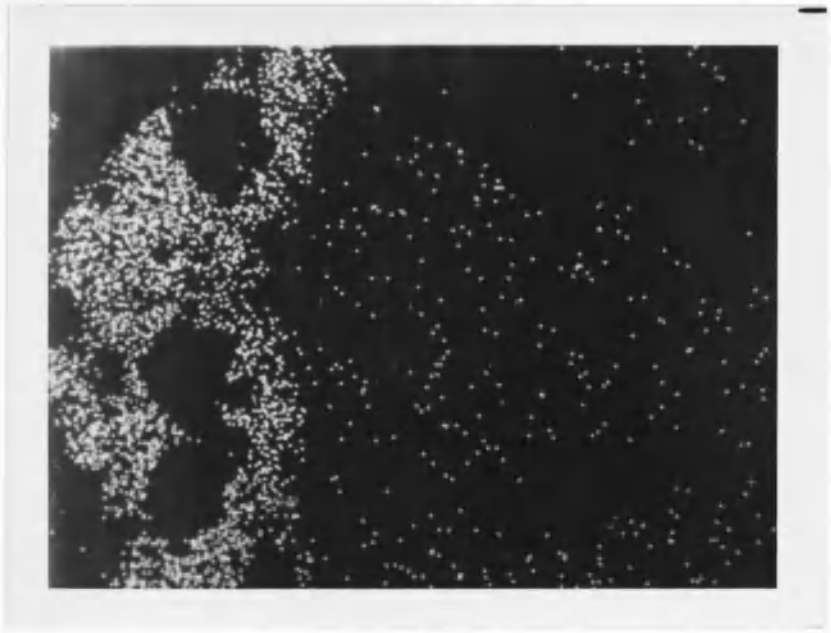

(a)

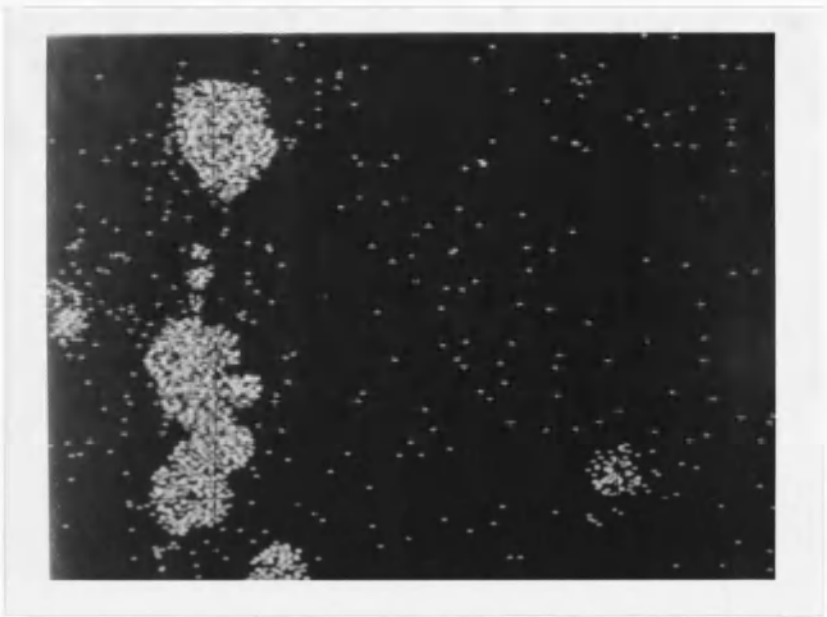

(b)

Fig. 21. Distribution of hafnium and nickel in the view shown in Fig. 20(a).

(a) Hafnium distribution.
(b) Nickel distribution. Notice the HfO_2 coating on the ZrO_2 surface and the nickel droplets within the HfO_2 coating. Magnification is 200x.

Table 19. Microprobe analysis of ZrO_2 crucible surface.

	K-Ratios		
	ZrO_2 crucible matrix	HfO_2 coating	Nickel-base metal droplets
Ni	< 0.001	< 0.001	0.91
Al	0.002	0.013	0.022
Hf	0.012	0.55	< 0.001
Ca	0.17	0.039	0.002
Si	< 0.001	< 0.001	0.006
Zr	0.66	0.038	< 0.001
O	0.23	0.23	0.009

during and after the pouring operation; the nickel had a slight tendency to wet the HfO_2 coating.

The HfO_2 layer on the ZrO_2 crucible appears to be a continuous, solid oxide layer. It is believed to be solid instead of porous because very little nickel (K-ratio < 0.001) was contained in this layer; the small amounts of aluminum, calcium, and zirconium are probably in the form of Al_2O_3, CaO, and MgO respectively.

Some Al_2O_3 was also noted on a section of the top surface of the bottom of the crucible. The microprobe results of this Al_2O_3 rich region along with a ZrO_2 crucible matrix sample are shown in Table 20. These data show that there is some Al_2O_3 on the surface of this crucible. Sutton and Green (1977) state that a continuous Al_2O_3 layer forms on the ZrO_2 crucible in which Ni-9.4Al is melted. It is believed that this Al_2O_3 formed in Melt 10 and was partly reduced by hafnium to form HfO_2

Table 20. Microprobe analysis of Al_2O_3-rich area on ZrO_2 crucible surface.

	K-Ratios	
	ZrO_2 crucible matrix	Al_2O_3-rich region
Ni	< 0.001	< 0.001
Al	0.003	0.24
Hf	0.012	0.076
Ca	0.17	0.18
Si	< 0.001	0.005
Zr	0.66	0.34
O	0.23	0.17

(Eq. 16) in Melts 11 and 12. Sutton and Maurer (1979) also stated that some Al_2O_3 formed on the crucible walls. Thus, it appears that on this ZrO_2 crucible surface, Al_2O_3 formed during Melt 10 and that this Al_2O_3 layer was reduced by the hafnium to form HfO_2 in Melts 11 and 12. However, most of the HfO_2 coating is believed to be formed by direct reduction of the ZrO_2 by the Hf in the melt as shown in the reaction below:

$$ZrO_2(s) + \underline{Hf} \rightarrow \underline{Zr} + HfO_2(s) \qquad (17)$$

It is predicted from thermodynamic consideration that this reaction goes toward the right (equilibrium constant > 1). Although no thermodynamic data for hafnium in nickel are available, it is known that pure HfO_2 is more stable than pure ZrO_2 at 1550°C as shown in Figure 2. Thus, it is assumed that the free energy of formation of HfO_2 in nickel base melts at 1550°C is lower (larger negative value) than the ΔG° for ZrO_2. Also, the activity of Hf (1% Hf in melts) is obviously much higher than the activity of Zr (initially no Zr in the melt). Also, Zr never has a chance to approach equilibrium because of the vacuum pump. By analyzing Eq. (2), it is clear that a negative value of ΔG would be obtained because both the ΔG° values and the activity values contribute towards a negative number. Thus, theoretical considerations predict the reduction of ZrO_2 by Hf in nickel base melts at 1550°C. This is backed up by these experimental results.

It is believed that this HfO_2 coating which forms on the ZrO_2 crucible serves to "condition" the crucible in that the HfO_2 coating is

much more chemically stable than the ZrO_2 crucible. It is theorized that a relatively inert HfO_2 crucible can effectively be made by melting hafnium-bearing nickel-base superalloys in a ZrO_2 crucible whereas a nominally pure HfO_2 crucible would be prohibitively expensive. Of course, further testing must be performed to determine the extent of HfO_2 coatings at various pressure levels, and oxygen analyses of subsequent melts must be made in order to check for the chemical stability of the HfO_2 coating.

On the surface of the Al_2O_3 crucible, an adherent, continuous nickel-base skull was found. Figures 22 and 23 show this skull on the Al_2O_3 crucible surface. Careful observation shows that the nickel rich metal is directly adjacent to the Al_2O_3 crucible surface. A layer of HfO_2 is present in the skull, but it does not appear that this HfO_2 directly coats the Al_2O_3 crucible surface as it does the ZrO_2 crucible surface. A careful comparison of Figures 22(a) and 23 must be made in order to see that this HfO_2 layer is not directly adjacent to the Al_2O_3 crucible surface. This observation agrees with the observation made by Sutton and Maurer (1979) who state that virtually no HfO_2 was attached to any crucible except their ZrO_2-Prefire crucible.

Microprobe analyses of various regions in this cross-sectional view of the Al_2O_3 crucible are given in Table 21. The relatively high K-ratio of nickel reported in the HfO_2 rich area suggests that this is HfO_2 dross which settled to the bottom of the nickel-base melt. It remains trapped in the solidified nickel-base skull metal after pouring.

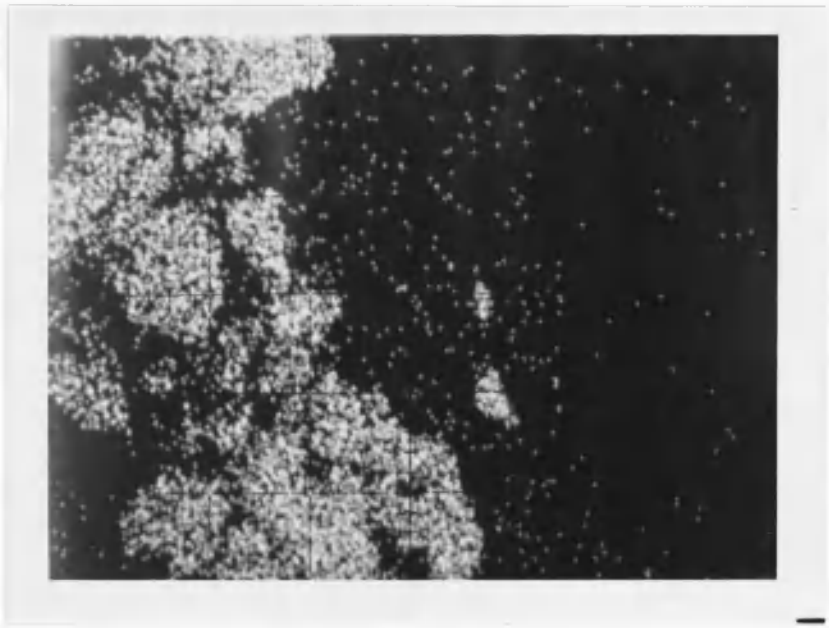

(a)

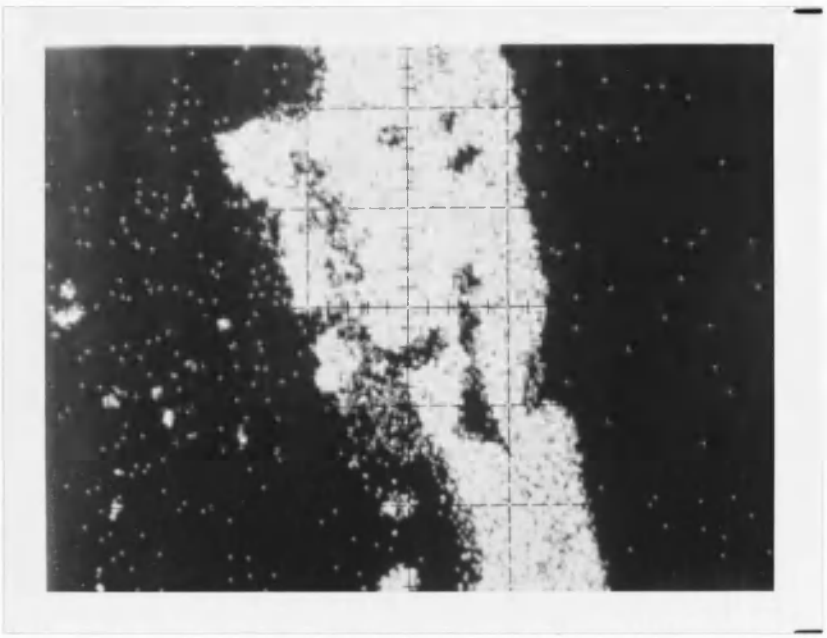

(b)

Fig. 22. Distribution of aluminum and nickel on the Al_2O_3 crucible (side view).

(a) Aluminum.
(b) Nickel. Notice that the nickel-base skull is directly adjacent to the Al_2O_3 crucible matrix. Magnification is 200x.

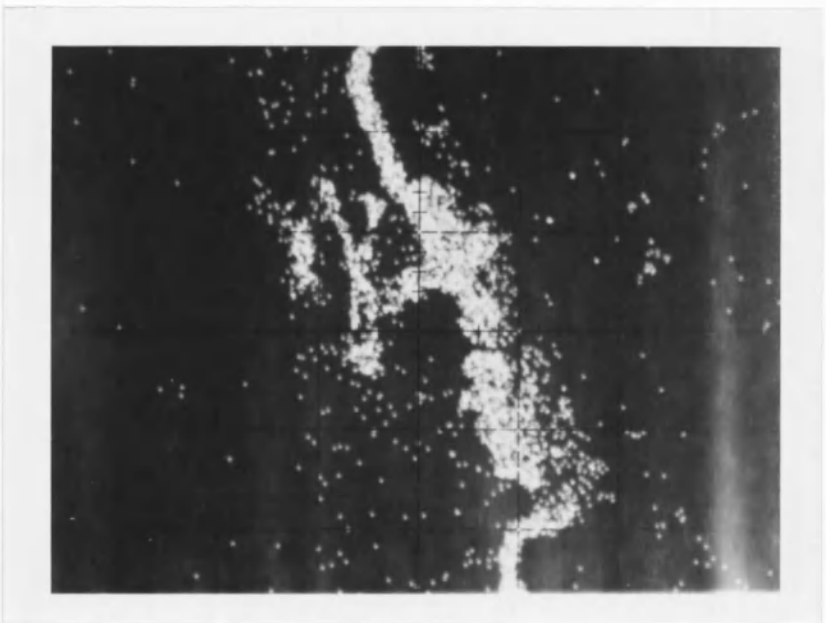

Fig. 23. Hafnium x-ray distribution on the Al_2O_3 crucible (side view).

Notice that most of this HfO_2 is within the nickel skull. Magnification is 200x.

Table 21. Microprobe analysis of HfO_2 and skull metal on Al_2O_3 crucible surface.

	K-Ratios		
	Al_2O_3 crucible matrix	HfO_2 coating	Nickel-base skull metal
Ni	0.005	0.67	> 1.0
Al	0.66	0.024	0.007
Hf	< 0.001	0.49	0.029
Ca	0.005	0.012	0.005
Si	0.012	0.022	0.046
Zr	< 0.001	0.006	< 0.001
O	> 1.0	0.16	0.010

It is theorized that the reason the skull is attached to the Al_2O_3 crucible surface is that the nickel-base metal tends to wet the crucible. In a sessile drop study by Sutton and Maurer (1979), the contact angle between their nickel-base alloy and their crucible was 78° which is very good wetting conditions. The skull is believed to have solidified on the crucible during and after pouring. It is so adherent to the crucible that it does not flow out with the majority of the melt during the pouring operation.

Sutton and Maurer (1979) also stated that a nickel-base skull layer was very adherent to their Al_2O_3-Prefire crucible. When this skull was peeled from their crucible, the surface grains were pulled away. A similar observation was noted when the skull was peeled from this Al_2O_3 crucible.

No definite proof of Al_2O_3 crucible decomposition was established by these probe results because of the 5% Al in two of the four melts makes it unclear whether any of the aluminum in the nickel base skull or ingots originated from the Al_2O_3 crucible. However, it is widely known that Al_2O_3 crucibles used to melt nickel-base alloys by vacuum induction melting do decompose to some slight extent. Vaughn and Geiger (1979), as well as Sutton and Maurer (1979), have made this observation.

Unfortunately, no decrease in the Al_2O_3 crucible decomposition rate in subsequent melts can be expected to occur due to this skull because this skull will probably simply remelt in the next heat. In other words, it is believed that this skull does not serve as a protective layer as the HfO_2 coating supposedly does on the ZrO_2 crucible.

Compared to the Al_2O_3 and ZrO_2 crucible surfaces, not much skull formation or oxide coating was noticed on the MgO crucible surface. Only small regions of Ni and Al_2O_3 were noticed adhering to the MgO surface as shown in Figures 24 and 25. Microprobe analyses of these phases on the MgO crucible is given in Table 22. It is probable that the aluminum x-ray distribution dots in Figure 25 represent Al_2O_3 adhering to the MgO crucible; this makes sense considering that spinel ($MgAl_2O_4$) is a very stable phase. Sutton and Maurer (1979) state that spinel is formed on the MgO crucible surface by the reactions:

$$2Mg(g) + 2Al_2O(g) + 3O_2(g) \rightarrow 2MgAl_2O_4(s) \qquad (22)$$

$$2Mg(g) + 2Al_2O_3(s) + O_2(g) \rightarrow 2MgAl_2O_4(s) \qquad (23)$$

Fig. 24. Nickel x-ray distribution image of an area on the MgO crucible surface.

Not much wetting of the surface was noticed. Magnification is 500x.

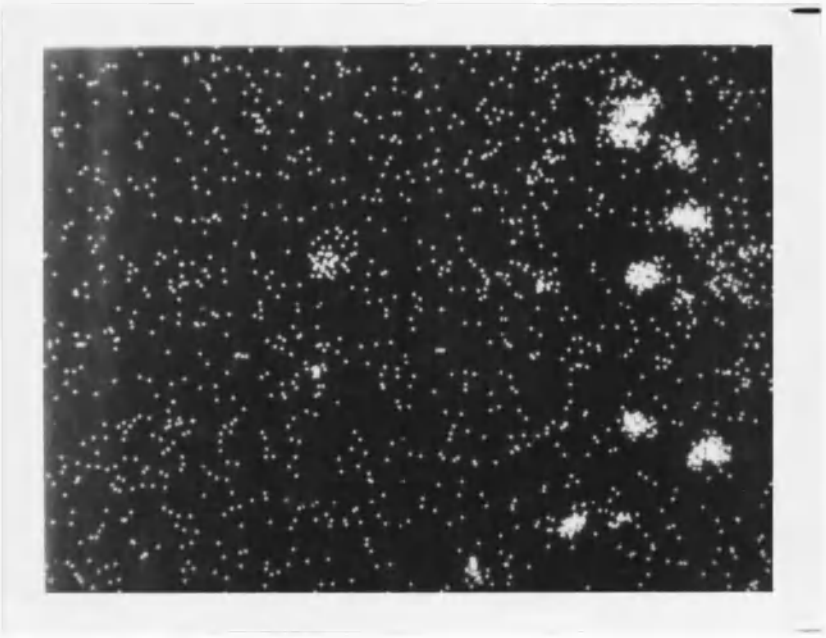

Fig. 25. Aluminum x-ray distribution image of an area on the MgO crucible surface.

Only small scattered spots form on this surface. Magnification is 500x.

Table 22. Microprobe analysis of MgO crucible surface.

	K-Ratios		
	MgO Matrix	Nickel-rich area	Al_2O_3-rich area
Ni	< 0.001	0.86	0.001
Al	0.002	0.004	0.45
Hf	< 0.001	< 0.001	< 0.001
Ca	0.009	0.005	0.012
Mg	> 1.0	< 0.001	0.011
Si	0.002	0.002	0.003
Zr	< 0.001	< 0.001	< 0.001
O	0.58	0.025	0.55

The probable reason for the lack of a skull or coating on the MgO crucible surface was the non-wetting characteristics of the alloy on the refractory. Sutton and Maurer (1979) studied the effect of contact angle as a function of crucible composition for a nickel-base alloy by performing sessile drop experiments. The alloy melted on a specimen from their MgO-Prefire crucible had the highest contact angle (θ = 144°, non-wetting) while their ZrO_2-Prefire and Al_2O_3-Prefire crucible had contact angles with the alloy of 100° and 78°, respectively.

4.8 Summary of Inclusion and Dross Forming Chemical Reactions

The information obtained from the ingot results are now combined with the information obtained from the crucible results to obtain an understanding of the chemical reactions which take place to cause harmful

primary inclusions and dross defects to form. This information is summarized in the three schematic diagrams (Figures 26-28) involving the three crucible systems. These diagrams show, in effect, the inclusion forming reactions taking place in the Ni-0.15C-5Al-1Hf melts. By ignoring the reactions involving the additions of aluminum and/or hafnium, the major reactions taking place in the other nine melts can be obtained.

In all three crucible systems, there are some reactions which are common; these are discussed first. Alumina and hafnium oxide inclusions form in all of these melts by the reaction of Al and Hf with available O. Alumina-rich dross rises to the top surface of the melt while hafnium oxide-rich dross tends to sink to the bottom of the melt. This is evident by analyzing the composition of the dross on the top and bottom surfaces of the ingots containing aluminum or hafnium or both. The just poured ingots remain molten long enough for appreciable quantities of the Al_2O_3 and HfO_2 rich dross phases to either float to the top or to sink to the bottom, respectively. Other constituents are also in these dross layers forming at the two surfaces depending on the crucible used. Some HfO_2 is present in the top dross layer while some Al_2O_3 is in the bottom dross layer. This probably occurs because Al_2O_3 and HfO_2 particles agglomerate to each other and either float or sink depending on the concentration of each oxide in the particular cluster. It is also predicted that Hf reacts with Al_2O_3 inclusions to form HfO_2 rich inclusions (Eq. 16) because hafnium has a much higher affinity for oxygen than aluminum does. The carbon in the melt reacts with oxygen to form CO near the melt surface where the metallostatic head is low enough for CO bubbles

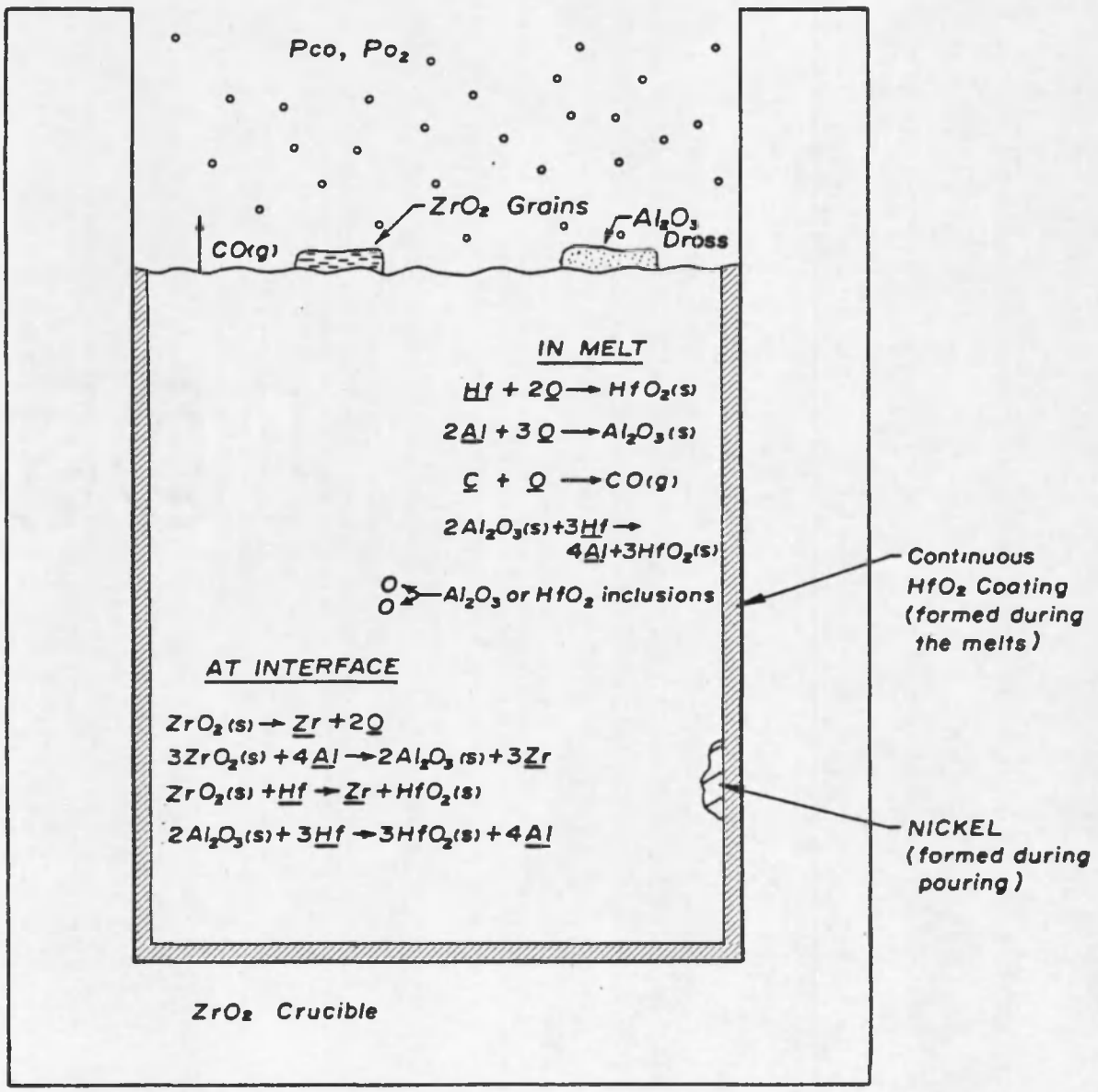

Fig. 26. Major chemical reactions within the ZrO_2 crucible systems.

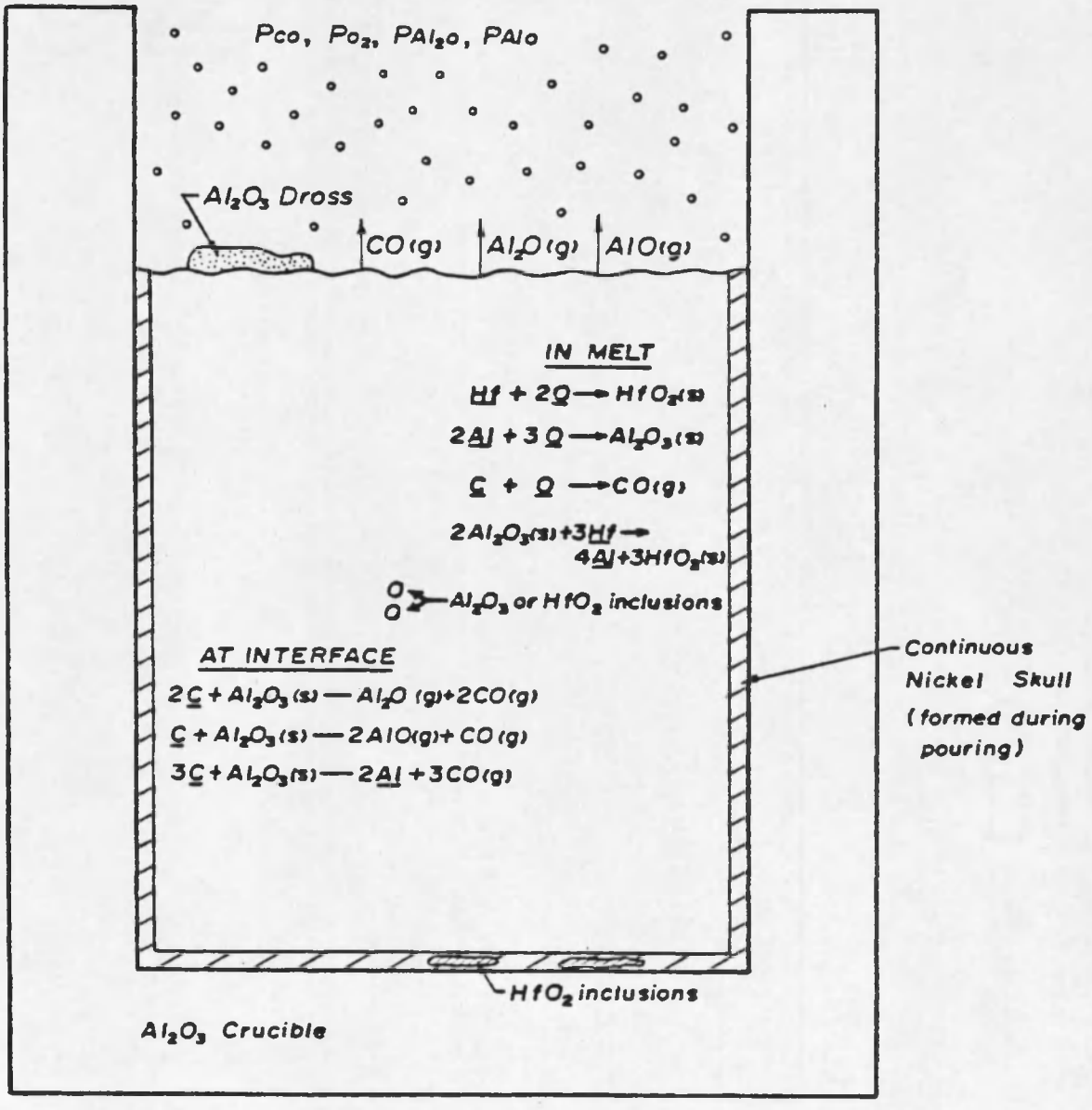

Fig. 27. Major chemical reactions within the Al_2O_3 crucible systems.

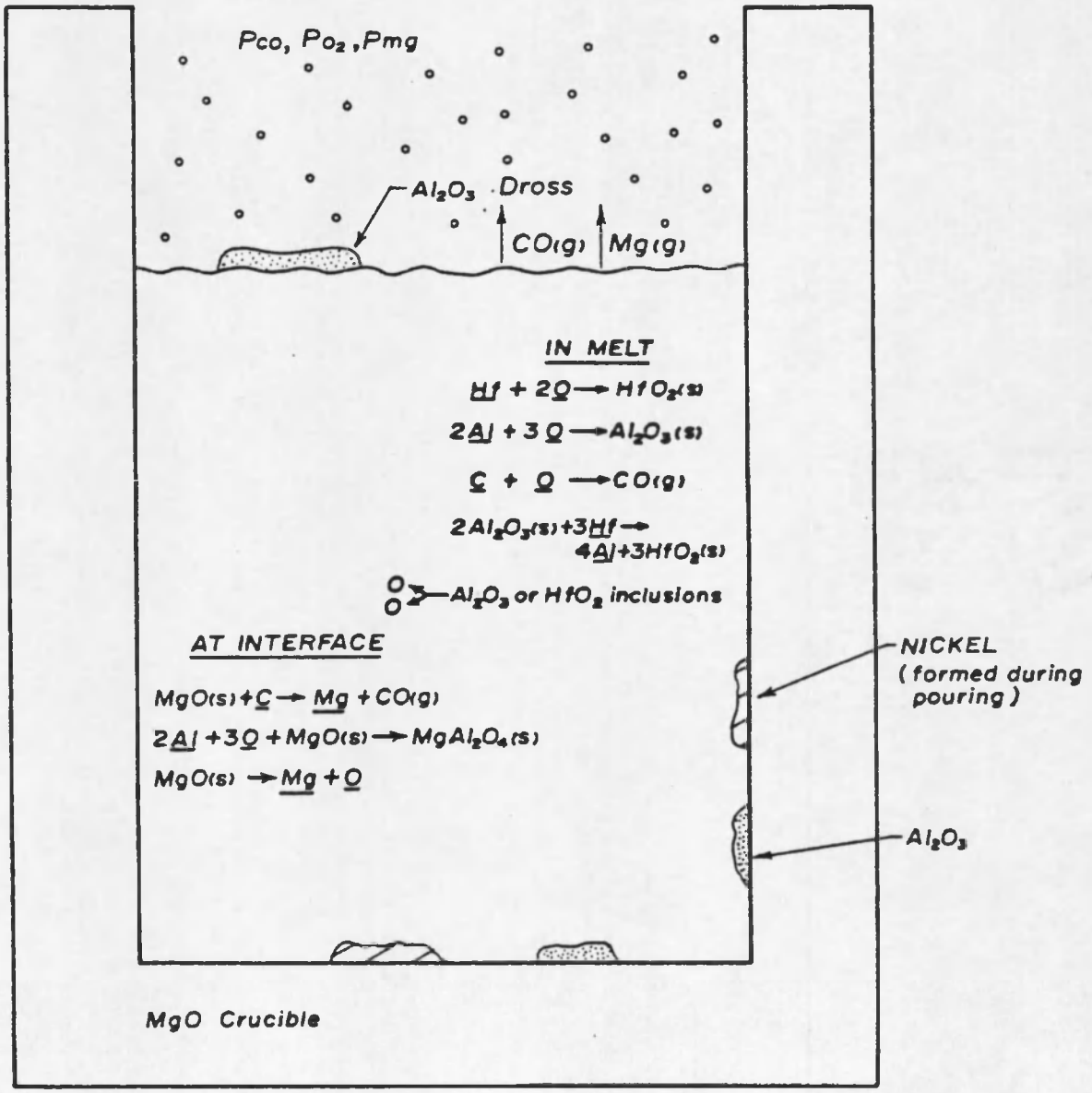

Fig. 28. Major chemical reactions within the MgO crucible systems.

to form. This CO reaction is beneficial in decreasing the amount of inclusions and dross defects because the CO leaves as a gas and decreases the amount of oxygen available to react with aluminum and hafnium.

Reactions peculiar to the ZrO_2 crucible system are now discussed; a schematic diagram, which shows the major reactions in the ZrO_2 crucible system, is shown in Figure 26. The dross on the top and bottom surfaces of the various ingots contain appreciable quantities of ZrO_2, CaO, and SiO_2. This is evidence of ZrO_2 crucible decomposition or reduction during melting. The aluminum, hafnium, and carbon in the melt all tend to reduce the ZrO_2 crucible. Alumina (Al_2O_3) forms on the ZrO_2 crucible matrix and also as a coating on the ZrO_2 grains on the top of Melt 10. Thus, some Al_2O_3 is believed to have formed on the ZrO_2 crucible surface during Melt 10 and perhaps during Melt 12 as well. In Melt 12, the hafnium may have reduced the ZrO_2 as well as any Al_2O_3 which may have been forming on the surface.

It has definitely been established that Hf reacts with the ZrO_2 to form a relatively thick (approximately 0.12mm) HfO_2 coating as seen in Figure 21(a). However, the pressure within the system during the two hafnium-bearing melts in the ZrO_2 crucible was 1-2 torr (1000-2000 microns) instead of the intended 1-10 microns used widely in industrial practice. It cannot be known for sure whether a much thinner HfO_2 coating would form when melting these hafnium-bearing nickel-base alloys under the customary 1-10 microns pressure. But Sutton and Maurer (1979) stated that appreciable amounts of HfO_2 formed on their ZrO_2-Prefire crucible when melting under 1-10 microns pressure. It is believed that

such a HfO_2 coating serves as a chemically stable and protective layer. Thus, it is theorized that subsequent melts will be cleaner because much less oxygen would be introduced into the melt when in contact with a HfO_2 refractory coating rather than ZrO_2, itself. However, further work should be done to substantiate this theory.

The ZrO_2 crucible is also reduced by carbon. This probably occurs only near the melt surface where the metallostatic head is low enough for CO bubbles to form. This Zr is free to react with additional O to form ZrO_2 and become part of the dross phase present in the ingot. The ZrO_2 crucible also self-decomposes to form Zr and O. This also increases the supply of O available to react with aluminum and hafnium to form inclusions and dross defects.

The major dross-forming reactions occurring in the Al_2O_3 crucible system are shown in Figure 27. The reactions within the melt, which form Al_2O_3, HfO_2, and gaseous CO, are shown in the figure and have previously been discussed. Considerable amounts of SiO_2 are also present in the dross phases. Although the major source of the silicon may have been from the original aluminum charge metal, it is possible that some of the Si may have come from the decomposing Al_2O_3 crucible.

It is well established that the Al_2O_3 crucible is reduced by carbon even though this could not be established from the microprobe results. The reaction products include $Al_2O(g)$, $AlO(g)$, Al, and $CO(g)$. Meadowcraft and Elliott (1963) state that the formation of these volatile suboxides under vacuum somewhat diminish the effectiveness of the substitution of Al_2O_3 crucible for a less inert crucible. In other words,

the oxygen leaves as a gas and is not available to react with Al or Hf and form inclusions or dross.

It is predicted from thermodynamics that Hf would reduce the Al_2O_3 and perhaps form a coating as it did on the ZrO_2 crucible surface. However, no HfO_2 coating has definitely been found on the Al_2O_3 crucible surface. The HfO_2 shown in Figure 23 does not seem to adhere to the Al_2O_3 crucible surface shown in Figure 22(a). Perhaps the reason for the lack of a noticeable HfO_2 formation was that the 5% Al in Melt 4 decreased the tendency for formation of HfO_2. Unfortunately, no thermodynamic data for hafnium in nickel-base melts are available so no rigorous calculations can be done. However, Sutton and Maurer (1979) state that virtually no HfO_2 formed on any of their crucibles (including the Al_2O_3-Prefire crucible) except their ZrO_2-Prefire crucible; all of their melts were made at pressures of 1-10 microns. Instead, a nickel skull is retained on the Al_2O_3 crucible after pouring. This skull is believed to be retained because of the good wetting conditions between the nickel-base alloy and the crucible as discussed earlier. This nickel-base skull is not believed to be a protective coating as the HfO_2 is suggested to be on the ZrO_2 crucible. It should simply remelt during the following melt and is not beneficial in decreasing the amount of Al_2O_3 crucible decomposition.

The major reactions which occur during melting in the MgO crucible system are summarized in Figure 28. Many of the reactions within these melts have already been discussed in connection with the ZrO_2 and Al_2O_3 crucible systems. In other words, aluminum-rich dross formed on the top surfaces and hafnium oxide-rich dross formed on the bottom surfaces of

the appropriate ingots. Considerable quantities of MgO, CaO, and SiO_2 were also present in the dross layers; these obviously come from the decomposing MgO crucible. Also, there is probably more MgO decomposition than is indicated by the quantities of MgO present in the dross because appreciable quantities of $Mg_{(g)}$ are believed to vaporize during the melting process. The Mg cannot compete with the Al and Hf for the available O so it vaporizes at the melt surface and enters the gas phase which is continuously pumped out of the system.

The MgO crucible can also be reduced by carbon according to reaction 7; this introduces Mg into the melt which is then free to react with available O to form MgO in the dross layer as well as form $Mg_{(g)}$. This fraction of the carbon which reacts with the MgO does not deoxidize the melt.

No appreciable metallic skull or oxide coating formed on the MgO crucible surface as it did on the Al_2O_3 and ZrO_2 crucible surfaces. However, small amounts of nickel and Al_2O_3 were noted to be scattered throughout the surface. The probable reason for the lack of a metallic skull or an oxide coating is the non-wetting conditions between the nickel-base alloys and the MgO crucible surface as discussed earlier. Thus, no protective layer, which would decrease the amount of oxygen pumped into the melt, forms on the MgO crucible surface.

CHAPTER 5

CONCLUSIONS AND RECOMMENDATIONS

Conclusions of this study include the following:

(1) Dross defects rich in hafnium oxide form on the bottom surfaces of nickel-base ingots containing 1% hafnium when poured from melts which are vacuum melted in the pressure range of 1-10 microns.

(2) Alumina-rich dross defects form on the top surfaces of nickel-base ingots containing 5% aluminum when poured from melts which are vacuum melted in the pressure range of 1-10 microns.

(3) An HfO_2 coating forms on the ZrO_2 crucible when melting hafnium-bearing nickel-base alloys under pressures of 1-2 torr. Hafnium reduces the ZrO_2 as well as any Al_2O_3 which previously formed on the ZrO_2 crucible. This HfO_2 coating is more chemically stable and thus this coating should decrease the amount of oxygen "pumped" into subsequent melts by crucible decomposition. Thus, it is believed that a more inert, relatively inexpensive HfO_2 crucible can effectively be made by melting hafnium-bearing nickel-base alloys in a ZrO_2 crucible. A nominally pure HfO_2 crucible would be prohibitively expensive.

(4) A very adherent nickel-base skull forms on the Al_2O_3 crucible. This skull is believed to be simply the nickel-base metal remaining in the crucible after pouring. This skull is adherent because the contact angle between the nickel-base alloys and the Al_2O_3 crucible is relatively low. No decrease in the Al_2O_3 crucible decomposition rate in subsequent

melts can be expected to occur because this nickel-base skull will simply remelt in future heats.

(5) No appreciable metallic skull or oxide coating formed on the MgO crucible. This is believed to be due to the relatively high contact angle between nickel-base alloys and MgO crucibles. Thus, no protective coating forms on the MgO crucible as it does on the ZrO_2 crucible. Appreciable evidence of MgO and ZrO_2 crucible decomposition was observed.

(6) This decomposition increases the amount of oxygen in the melt. No positive proof of Al_2O_3 crucible decomposition was observed although it is probable that Al_2O_3 crucibles decompose slightly.

It is recommended that more work be done on analyzing for HfO_2 coatings on a ZrO_2 crucible. The effect of pressure on the thickness of the HfO_2 coating should be analyzed. It should also be determined whether this HfO_2 coating causes subsequent melts to be much cleaner.

Further work can be done on analyzing the rate of crucible decomposition as a function of pressure in order to establish an optimum melting pressure. This could be done by performing a more quantitative study of inclusion size and composition as well as decomposition products (ex., MgO, ZrO_2, CaO, SiO_2, etc.) in the ingots when melting under various pressures.

The size distribution as well as the morphology of the various oxide inclusions as a function of alloy composition, crucible, and pressure should also be studied; these factors heavily influence the fatigue strength of castings.

APPENDIX A

MELT DATA

Tables A-1 to A-12 contain data recorded during the melting and pouring of the twelve nickel-base melts.

Table A-1. Record of Melt 1.

Alloy: Ni-0.15C
Crucible: Al_2O_3
Previous Heats in Crucible: None

Weights of Charge Materials

1447.8 g Ni
2.17 g C

Time (minutes)	Observations or Events
	1 micron
0	Turned power on to 14 kW.
5	4 microns
9	4 microns
13	5 microns
15	1475°C Metal is molten.
16	9 microns
17	1530°C
18	1550°C
19	Turned power off and poured melt at 12 microns.

Table A-2. Record of Melt 2.

Alloy: Ni-0.15C-5Al
Crucible: Al_2O_3
Previous Heats in Crucible: Melt 1

Weights of Charge Materials

1327.9 g Ni
68.5 g Al
2.10 g C

Time (minutes)	Observations or Events
	2 microns
0	Turned power on to 14 kW.
4	3 microns
8	4 microns
12	5 microns
15	1470°C Metal is molten.
17	7 microns
18	1540°C
19	1555°C
20	Turned power off and poured melt at 9 microns.
	Scum layer noticed on top of the solidifying ingot.

Table A-3. Record of Melt 3.

Alloy: Ni-0.15C-1Hf
Crucible: Al_2O_3
Previous Heats in Crucible: Melts 1 and 2

Weights of Charge Materials

1370.5 g Ni
2.10 g C
27.9 g Hf

Time (minutes)	Observations or Events
	1 micron
0	Turned power on to 14 kW.
3	2 microns
5	2 microns
7	2 microns
9	3 microns
11	3 microns
13	1450°C Metal is molten.
15	5 microns Dross layer noticed on the top surface of the melt.
17	5 microns
	1565°C
18	Turned power off and poured melt at 7 microns.

Table A-4. Record of Melt 4.

Alloy: Ni-0.15C-5Al-1Hf
Crucible: Al_2O_3
Previous Heats in Crucible: Melts 1, 2, and 3

Weights of Charge Materials

1126.3	g Ni
1.81	g C
61.4	g Al
13.9	g Hf

Time (minutes)	Observations or Events
	1 micron
0	Turned power on to 14 kW.
2	3 microns
4	3 microns
6	3 microns
8	3 microns
10	4 microns
12	4 microns
14	1455°C Metal is molten.
17	4 microns
	1550°C
18	Turned power off and poured melt at 5 microns.
	Scum layer noticed on top of the solidifying ingot.

Table A-5. Record of Melt 5.

Alloy: Ni-0.15C
Crucible: MgO
Previous Heats in Crucible: None

Weights of Charge Materials

1298.0 g Ni
1.95 g C

Time (minutes)	Observations or Events
	.9 microns
0	Turned power on to 14 kW.
1	1 micron
3	2 microns
5	3 microns
7	5 microns
9	5 microns
11	20 microns
13	50 microns
14	1460°C Metal is molten.
17	1545°C
18	Turned power off and poured melt at 200 microns.

Table A-6. Record of Melt 6.

Alloy: Ni-0.15C-5Al
Crucible: MgO
Previous Heats in Crucible: Melt 5

Weights of Charge Materials

1185.6 g Ni
62.5 g Al
1.87 g C

Time (minutes)	Observations or Events
	1 micron
0	Turned power on to 14 kW.
4	1 micron
5	2 microns
6	4 microns
11	1470°C Metal is molten.
12	Power cut to 6 kW.
13	5 microns
15	1450°C
18	5 microns
25	6 microns
31	Turned power off.
33	Visual dross layer noticed near the crucible walls.
38	Turned power back on to 14 kW.
40	1525°C
42	1550°C
	Turned power off and poured melt at 12 microns.
	Scum layer noticed on top of the solidifying ingot.

Table A-7. Record of Melt 7.

Alloy: Ni-0.15C-1Hf
Crucible: MgO
Previous Heats in Crucible: Melts 5 and 6

Weights of Charge Materials

1235.1 g Ni
1.88 g C
36.4 g Hf

Time (minutes)	Observations or Events
	.9 microns
0	Turned power on to 14 kW.
4	1 micron
6	2 microns
10	4 microns
18	4 microns
19	1440°C
	It was noticed that when a solidified portion of metal near the top of the crucible remelts, dross comes out of this remelted metal.
22	1535°C
23	6 microns
24	1545°C
25	Turned power off and poured melt at 8 microns.

Table A-8. Record of Melt 8.

Alloy: Ni-0.15C-5Al-1Hf
Crucible: MgO
Previous Heats in Crucible: Melts 5, 6, and 7

Weights of Charge Materials

1127.4	g Ni
1.80	g C
64.0	g Al
17.9	g Hf

Time (minutes)	Observations or Events
	1 micron
0	Turned power on to 14 kW.
1	2 microns
4	2 microns
5	930°C
7	3 microns
9	4 microns
13	1465°C Metal is molten.
15	4 microns
16	1545°C
	Scum layer noticed forming on the top of the melt.
17	4 microns
18	Turned power off and poured melt at 4 microns
	Scum layer noticed on top of the solidifying ingot.

Table A-9. Record of Melt 9.

Alloy: Ni-0.15C
Crucible: ZrO_2
Previous Heats in Crucible: None

Weights of Charge Materials

1198.7 g Ni
1.80 g C

Time (minutes)	Observations or Events
	1 micron
0	Turned power on to 14 kW.
1	1 micron
5	2 microns
8	1100°C
9	3 microns
11	1200°C
13	4 microns
15	1480°C Metal is molten.
18	1535°C
19	Turned power off and poured melt at 5 microns.

Table A-10. Record of Melt 10.

Alloy: Ni-0.15C-5Al
Crucible: ZrO_2
Previous Heats in Crucible: Melt 9

Weights of Charge Materials

1045.3 g Ni
55.7 g Al
1.80 g C

Time (minutes)	Observations or Events
	2 microns
0	Turned power on to 14 kW.
1	2 microns
2	2 microns
5	1200°C
6	2 microns
8	2 microns
9	1450°C Metal is molten.
11	3 microns
12	1545°C
13	Turned power off and poured melt at 4 microns.
	Scum layer noticed on top of the solidifying ingot.

Table A-11. Record of Melt 11.

Alloy: Ni-0.15C-1Hf
Crucible: ZrO_2
Previous Heats in Crucible: Melts 9 and 10

Weights of Charge Materials

1194.3 g Ni
13.7 g Hf
1.80 g C

Time (minutes)	Observations or Events
	0.95 torr (1 torr equals 1000 microns)
0	Turned power on to 14 kW.
2	1.0 torr
4	1.1 torr
7	1.1 torr
9	1.4 torr
12	1475°C Metal is molten.
	Particles collect on the top surface of the melt and travel toward the crucible walls.
14	1525°C
16	1550°C
17	Turned power off and poured melt at 1.2 torr.
	Scum layer noticed on top of the solidifying ingot.

Table A-12. Record of Melt 12.

Alloy: Ni-0.15C-5Al-1Hf
Crucible: ZrO_2
Previous Heats in Crucible: Melts 9, 10, and 11

Weights of Charge Materials

1128.6 g Ni
60.7 g Al
18.3 g Hf
1.80 g C

Time (minutes)	Observations or Events
	1.0 torr (1 torr equals 1000 microns)
0	Turned power on to 14 kW.
2	1.05 torr
4	1.10 torr
7	1.10 torr
10	1.20 torr
13	1460°C Metal is molten.
16	2 torr
17	1590°C
19	Greater than 2 torr pressure.
20	1625°C
21	Turned power off and poured melt above 2 torr.
	Thick oxide skin formed on the entire top surface of the melt.

LIST OF REFERENCES

Cremisio, R.: The Superalloys, Edited by R. Sims and W. Hagel, John Wiley & Sons, New York, 1972, p. 373.

Fawley, R.: The Superalloys, Edited by R. Sims and W. Hagel, John Wiley & Sons, New York, 1972, p. 3.

Flemings, M.: Solidification Processing, McGraw-Hill, New York, 1974, p. 196.

Harris, K., R. Schwer, G. Brown, and D. Valentine: Proceedings of Vacuum Metallurgy Conference, 1977, p. 2.

Hockin, J.: Superalloys - Processing, American Institute of Mining, Metallurgical, and Petroleum Engineers, 1972, p. C-1.

Marder, J.: "Characterization of Casting Defects in Typical Castings of a Directionally Solidified Superalloy," TRW Final Report, AFML Contract F33615-76-C-5373, 1979.

Meadowcraft, T., and J. Elliott: Transactions of Vacuum Metallurgy Conference, 1963, p. 1.

Mosier, J.: "Materials for Advanced Turbine Engine Review," presented at NASA-Lewis Research Center, Cleveland, Ohio, March 29, 1978.

Rosenqvist, T.: Principles of Extractive Metallurgy, McGraw-Hill, New York, 1974.

Sakakibara, M., and S. Sekino: Superalloys - Processing, American Institute of Mining, Metallurgical, and Petroleum Engineers, 1972, p. I-1.

Schlatter, R.: Superalloys - Processing, American Institute of Mining, Metallurgical, and Petroleum Engineers, 1972, p. A-1.

Sigworth, G., J. Elliott, G. Vaughn, and G. Geiger: Canadian Met. Quarterly, Annual Volume 1977, p. 104.

Snape, E., and P. Beeley: Journal of the American Ceramic Society, 1967, Vol. 50, p. 349.

Sutton, W., and D. Green: Ceramic Microstructures '76, Westview Press, Boulder, Colorado, 1977, p. 520.

Sutton, W., and G. Maurer: Proceedings of Sixth Vacuum Metallurgy Conference, Edited by G. Bhat and R. Schlatter, 1979, p. 340.

Vaughn, G., and G. Geiger: Proceedings of 6th International Vacuum Metallurgy Conference, Edited by G. Bhat and R. Schlatter, 1979, p. 357.